

MANTLE ORIGIN OF THE ANTRONA SERPENTINITES (ANTRONA OPHIOLITE, PENNINE ALPS) AS INFERRED FROM MICROSTRUCTURAL, MICROCHEMICAL, AND NEUTRON DIFFRACTION QUANTITATIVE TEXTURE ANALYSIS

Paola Tartarotti^{*✉}, Michele Zucali^{*◦}, Matteo Panseri^{*}, Sabrina Lissandrelli^{**}, Silvia Capelli^{***}
and Bachir Ouladdiaf^{***}

^{*} Dipartimento di Scienze della Terra “Ardito Desio”, Università degli Studi di Milano, Italy.

^{**} Via G. Marconi 66, 28844 Villadossola, Italy.

^{***} Institut Laue-Langevin, Grenoble, France.

◦ CNR-IDPA, Sezione di Milano, Italy.

✉ Corresponding author: e-mail: paola.tartarotti@unimi.it

Keywords: Antrona ophiolite, serpentinite, mantle peridotite, neutron diffraction, Quantitative texture analysis. Pennine Alps.

ABSTRACT

The Antrona ophiolite is located in the Italian side of Western Central Alps. In the Alpine nappe stack, it lies at low structural levels, being sandwiched between the overlying continental Monte Rosa Nappe (upper Penninic) and the underlying Camughera-Moncucco continental Unit (middle Penninic). The ophiolite sequence includes serpentinitized ultramafites, metagabbros and mafic rocks covered by calcschists. The ultramafic portion of the Antrona ophiolite consists of serpentinitized peridotites, with interbedded layers of various mafic/ultramafic rocks, and underlies the mafic rocks and metasediments. In spite of the Alpine tectonic and metamorphic evolution of the Antrona ophiolite and its heavy serpentinitization, the ultramafic rocks preserve relict texture and mineralogy that allow discussing the nature of their protoliths. Olivine-clinopyroxene-spinel-bearing serpentinites still retain relict porphyroclastic texture, commonly attributed to mantle peridotites. This inference is supported by quantitative textural analysis of Lattice Preferred Orientation by neutron diffraction, performed for the first time in olivine crystals of Alpine ophiolites, suggesting T conditions > 800°C for the activation of slip systems. Mineral chemistry of fresh olivine, clinopyroxene and spinel also contribute to support the mantle nature of the serpentinite protolith. The Antrona ophiolite may thus be regarded as a fossilized fragment of oceanic lithosphere including mantle rocks, volcanics and deep-sea sediments. Although their extension is smaller, the Antrona ophiolite seems to be comparable with a coherent ophiolitic slice, such as Zermatt Saas ophiolite more than with a serpentinite mélange.

INTRODUCTION

The Antrona ophiolite represents remnants of the oceanic lithosphere of the Mesozoic Western Tethys, now inserted as tectonic slices in the Penninic nappe pile of the western Central Alps. The Alpine tectono-metamorphic evolution of this ophiolite is characterized by subduction-related blueschist prograde path, followed by high-pressure (eclogitic) metamorphic peak, and subsequent retrograde exhumation dominated by epidote-amphibolite to amphibolite facies conditions (Colombi and Pfeifer, 1986; Pfeifer et al., 1989; Carrupt and Schlup, 1998; Turco and Tartarotti, 2006). As some ophiolites of the Western Alps (e.g., Zermatt-Saas Unit) the Antrona ophiolite still retains well-preserved portions of the oceanic lithosphere. One of the main discussion recently developed on the Western Alps ophiolites regards their internal tectonic setting, which is considered crucial for understanding the subduction dynamics. Namely, two main settings have been recognized: one represents serpentinite mélanges consisting of tectonic ophiolitic blocks inserted in a serpentinite matrix, and showing a wide range of P-T conditions (e.g., Monviso, Voltri, Blake et al., 1995; Guillot et al., 2004; Federico et al., 2007); the other represents relatively coherent tectonic slices with km-scale length and thickness, and showing almost homogeneous burial and exhumation patterns (e.g., Zermatt-Saas ophiolite, Angiboust et al., 2009; 2011; Monviso ophiolite, according to Lombardo et al., 1978; Castelli and Lombardo, 2007; Angiboust et al., 2011). All the mentioned ophiolites have been interpreted as deriving from subduction and exhumation of the Tethyan Ocean

which has been regarded as a slow-spreading realm, comparable to the modern Atlantic Ocean (e.g., Lagabriele and Cannat, 1990; Lagabriele and Lemoine, 1997; Tartarotti et al., 1998). The internal setting of the Antrona ophiolite is still not well constrained, probably due to its small extent and pervasive metamorphic retrogression. Consequently, this ophiolite is often neglected and poorly considered for paleogeographic reconstruction of the Western Tethys.

In this paper, we focused our study on the ultramafic rocks of the Antrona ophiolite by performing original geological field mapping and sampling, then integrated with microstructural and microchemical analyses. No published geological maps are available in literature, with the exception of the Geological Sheet Nb. 15 “Domodossola” at scale of 1:100.000 (Carta Geologica d’Italia, 1959). The studied samples are poorly serpentinitized olivine-rich rocks and dunites which still retain mineralogical and textural relics that allow discussing and interpreting their primary characters and inferring the rock protolith. Microstructural and microchemical investigations were complemented by a quantitative texture analysis (LPO) by neutron diffraction on selected olivine-rich samples, in order to investigate the internal fabric of relict fresh olivine. The results allow discussing the active slip systems during the rock deformation and relating them with a mantle origin.

The aim of this paper was therefore to investigate the nature of the ultramafic rocks of the Antrona ophiolite, in order to shed light on the internal setting of this ophiolite sequence, and to improve a comparison with other ophiolites of the Alps.

GEOLOGICAL SETTING

Regional geology

The study area is located in the Pennine Alps, west of the Lepontine dome and SE of the Simplon Line (western part of the Central Alps; Fig. 1) where huge crystalline massifs are mantled by tectonic slices of ophiolite (e.g., Escher et al. 1987; 1993). In the internal Pennine Domain, the Zermatt-Saas ophiolite wraps the upper Penninic Monte Rosa Nappe and disappears below the middle Penninic Mischabel back-fold; the Antrona ophiolite lies on the footwall of the Monte Rosa Nappe and in turn overlays the middle Penninic Camughera-Moncucco Nappe (Beaith, 1956; Laduron, 1976; Bigioggero et al., 1981; Keller et al., 2005a). The Monte Rosa Nappe is a large NW-vergent recumbent anticline, strongly refolded by S-vergent backfolds of supposed Oligocene age (Milnes et al., 1981; Escher et al., 1997; Steck et al., 1997). Together with the Gran Paradiso and the Dora Maira “massifs”, the Monte Rosa Nappe is part of the inner and upper continental nappe system of the Penninic Zone in the Western Alps (Argand, 1911); it consists of pre-Alpine high grade paragneisses rich in mid- to coarse-grained pegmatites (Beaith, 1952; Gosso et al., 1979; Dal Piaz, 1993; Keller and Schmid, 2001; Keller et al., 2005b; see also review in Dal Piaz, 2001) and of a granitic complex of Late Carboniferous and Permian ages (Hunziker, 1970; Frey et al., 1976). During the Alpine orogeny, the pre-granitic high grade rocks were reworked into garnet micaschists and albitic schists, and the granitic bodies into foliated, schistose or mylonitic orthogneisses. The Antrona ophiolite is separated from the Monte Rosa basement by the Furgg Zone (Argand’s “synclinal de Furggen”; Argand, 1911). The Furgg Zone (Fig. 1) is made of micaschists, albitic schists, and leucocratic gneisses (Permian-Carboniferous) with eclogitic to greenschist-facies mafic boudins, thin micaceous quartzites and dolomitic marbles of probable pre-Mesozoic age (Beaith, 1954). In the upper part, the Furgg Zone includes tectonically transposed layers of Mesozoic

metasediments (tabular quartzites, dolostones, carnieuls, calcschists) as well as ophiolites of the underlying Antrona Unit (Blumenthal, 1952; Beaith, 1957; Dal Piaz, 1966; Wetzel, 1972). According to Dal Piaz’s studies, the Furgg Zone exposed in the southern Monte Rosa sectors has a pre-granitic protolith, is free of Mesozoic rocks, and is affected by eclogitic to greenschists facies Alpine metamorphism (Dal Piaz, 1964; 1966). More recently, the Furgg Zone has been regarded as the cover of the Monte Rosa basement (Jaboyedoff et al., 1996; Escher et al., 1997; Steck et al., 2001) or of the continental Portjengrat Unit (Keller and Schmid, 2001). Alternatively, the Furgg Zone has been considered as the suture of the Valais basin (Froitzheim, 1997; 2001) or a tectonic mélangé interposed between the continental Monte Rosa-Portjengrat Units and the Zermatt-Saas and Antrona ophiolites (Kramer, 2002). The Monte Rosa Nappe, the Furgg Zone, the Camughera Moncucco Unit, and the Zermatt-Saas and Antrona ophiolite have all experienced regional subduction-related high-pressure metamorphism during the Alpine orogeny (Dal Piaz et al., 1972; Compagnoni et al., 1977; Ernst and Dal Piaz, 1978; Colombi and Pfeifer, 1986; Dal Piaz and Lombardo, 1986; Borghi et al., 1996; Michard et al., 1996; Keller et al., 2005a; 2005b; Turco and Tartarotti, 2006). The Zermatt-Saas ophiolite subduction history is attested by the occurrence of lozenge-shaped pseudomorphs and other prograde relics followed by climax eclogitic to UHP mineral assemblage (Ernst and Dal Piaz, 1978; Oberhansli, 1980; Barnicoat and Fry, 1986; Martin and Tartarotti, 1989; Reinecke, 1991; 1998; Bucher et al., 2005; Angiboust et al., 2009). The eclogite facies metamorphism in the Zermatt-Saas Unit occurred during the Tertiary (Bowtell et al., 1994; Amato et al., 1999; Dal Piaz et al., 2001). Eclogite rocks in the Antrona ophiolite have been documented by Colombi and Pfeifer (1986) and Turco and Tartarotti (2006). During decompression accompanying the exhumation history, the Zermatt-Saas and upper Monte Rosa Units were re-equilibrated under greenschist facies conditions (Frey et al., 1974;

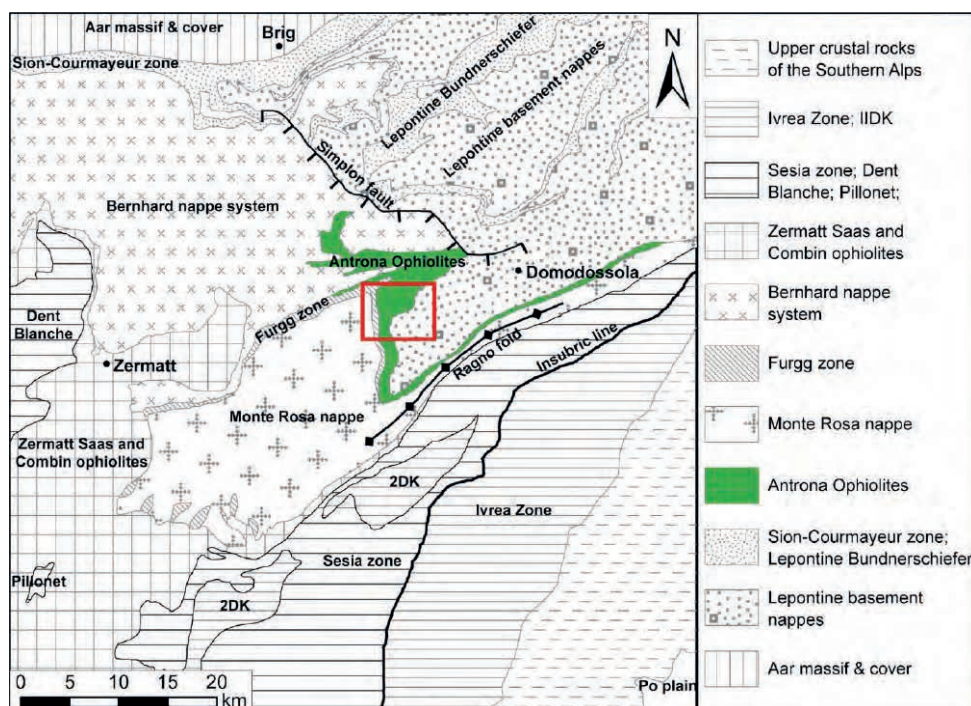


Fig. 1 - Tectonic map of the North-eastern Pennine Alps with location of the Antrona ophiolite and the study zone (boxed area). (Modified after Froitzheim, 2001).

Ernst and Dal Piaz, 1978; Keller et al., 2005a); differently, the lower parts of Monte Rosa and the Antrona ophiolite underwent amphibolite facies metamorphism during exhumation (Pfeifer et al., 1989; Turco and Tartarotti, 2006).

Geology of the Antrona ophiolite

The Antrona ophiolite is exposed on the Italian side of the western Central Alps between the Antrona, Loranco and Anzasca Valleys and in the Bognanco Valley (north-east of Antrona) and in the Vigezzo Valley, to the east of Domodossola; on the Swiss side, the Antrona ophiolite occurs in the Laggintal-Simplon area (Fig. 1). The Antrona ophiolite marks two of the most striking large-scale structures of the Central Alps: the Antrona synform (or Gabbio synform) attributed by Milnes et al. (1981) to the Mischabel-phase structures (regional phase 3), and the Vanzone antiform which pertains to the regional phase 4 (Milnes et al., 1981). Serpentinized ultramafites, metagabbros and mafic rocks constitute the main lithologies of the Antrona ophiolite as described by Laduron and Merlin (1974), Laduron (1976), Colombi and Pfeifer (1986), Colombi (1989), Pfeifer et al. (1989). Turco and Tartarotti (2006) report the occurrence of relict magmatic structures, such as pillow lavas and pillow breccias. Ophiolitic sections consisting of N-MORB to T-MORB-type metabasalts, minor serpentinites, and gabbros have been described in the Bognanco Valley by Carrupt and Schlup (1998); they are covered by, from bottom to top, garnet-micaschists, metaradiolarites (with metabasalts), calc-schists and intercalated metabasites, sedimentary breccias, calcschists, marbles, and graphitic marbles.

On the basis of mineral assemblages found for the first time in the Antrona ophiolite, such as lawsonite pseudomorphs within amphibolites, Turco and Tartarotti (2006) proposed a qualitative P-T evolution characterized by early Alpine prograde blueschist path followed by a high pressure (eclogitic) metamorphic peak. Mafic eclogites containing garnet, symplectites, amphibole and relict omphacitic clinopyroxene have been described by Colombi and Pfeifer (1986) in the Antrona-Anzasca area. P-T estimates for the metamorphic peak give $T = 372^{\circ}\text{C}$ for $P = 1 \text{ GPa}$ and $T = 386^{\circ}\text{C}$ for $P = 1.5 \text{ GPa}$ (Turco and Tartarotti, 2006). According to Turco and Tartarotti (2006), the retrograde path is dominated by epidote amphibolite to amphibolite facies conditions of Tertiary age.

STRUCTURAL ANALYSIS OF THE ANTRONA OPHIOLITE ULTRAMAFIC ROCKS

Field occurrence

The studied ultramafic portion of the Antrona ophiolite is exposed in the lower Loranco valley, near the village of Antronapiana where it forms a ca. 35 km² wide massif, extended from Antronapiana to Pizzo Ciapè (Fig. 2). These rocks underlie amphibolites and metasediments (Fig. 2b, c), thus constituting a sole for the volcanic and cover part of the Antrona ophiolite. In the marginal parts of the ultramafic massif, i.e., near Pizzo Ciapè, to the north, and in the southernmost part, the ultramafites are in contact with mafic rocks mostly represented by flaser metagabbros (Fig. 2b). This latter gradually changes to mylonitic amphibolite near the main tectonic contact with the Camughera-Moncucco Unit, here consisting of orthogneiss. Given the pervasive transposition produced during the Alpine tectonics, the con-

tacts between different lithologies are considered tectonic.

The ultramafic rocks are represented by foliated to mylonitic serpentinites mainly consisting of serpentine (antigorite) and magnetite. At the outcrop scale, serpentinite shows a thick alteration coat with a light-brown, ochre or reddish colour, whereas the fresh-fracture surface has a different colour depending on the rock texture. Magnetite occurs as 1-2 mm-sized isolated grains or as fine-grained aggregates elongated parallel to the rock foliation (Fig. 3a). Foliated serpentinite is black to dark green and often includes mm- to cm-sized fine-grained boudins or layers infolded or transposed within the rock foliation and characterized by various shape and colour. Due to their fine grain-size, the composition of these layers cannot be easily defined in the field, thus a petrographic analysis is necessary for their characterization (see later). The following types of rocks interbedded within serpentinite were distinguished in the field: a) millimetric brownish ol+cpx-layers (Table 1a); b) millimetric boudins or lozenge-shaped cpx + am ± chl ± mag-aggregates (Fig. 3b and Table 1b); c) centimetric white-to-greenish cpx-rich layers transposed within the serpentinite foliation (Fig. 4a and Table 1c).

Other rocks associated with foliated or slightly foliated serpentinites are dunites, amphibole-rich rocks, and chloriteschists. Dunites occur as dm-thick layers or pods parallel to the serpentinite foliation. The amphibole-rich rocks form dm-thick and few meters-long layers concordant with the serpentinite foliation (Fig. 4b and Table 1d). The rock is massive due to the fine grain-size and black in colour; it is commonly surrounded by centimetric chloriteschist layers showing sharp contacts against the serpentinite. Chloriteschists also occur as isolated layers within the serpentinites or associated to amphibole+chlorite-rich layers.

Mylonitic serpentinite has a light green colour and is characterized by a pervasive foliation. This type of rock often includes sub-millimetric rounded or lens-shaped porphyroblasts made of Ca-carbonate.

Mesostructural analysis

Four main deformational phases were recognized (Table 1): D_1 and D_2 produced the most pervasive foliations at the scale of the outcrops, while D_3 produced gentle folding of the pre-existing structures such as S_1 , D_2 folds, and S_2 . D_4 is characterized by diffuse fracturing and faults.

$D_1 + D_2$ phases

Two main foliations (S_1 and S_2) related to different stages of the Alpine evolution were recognized in the field (Table 1). S_1 occurs only locally and is mainly recorded by the brownish ol + cpx-layers and by the white/greenish cpx-rich layers infolded in the serpentinite and forming tight or isoclinal folds (mostly detectable under the microscope) within the S_2 foliation. D_2 deformation is responsible for isoclinal folding of S_1 (Table 1a) and the development of the S_2 foliation, mainly defined by antigorite and magnetite (Fig. 3). However, D_2 folds described by pyroxene-rich and amphibole-rich layers do not always develop an axial plane foliation.

In the marginal parts of the ultramafic massif (see Fig. 2) the contact between serpentinites and mafic rocks is marked by D_2 mylonitic serpentinites and minor chloriteschists.

D_3 phase

S_1 and D_2 structures have been overprinted by D_3 defor-

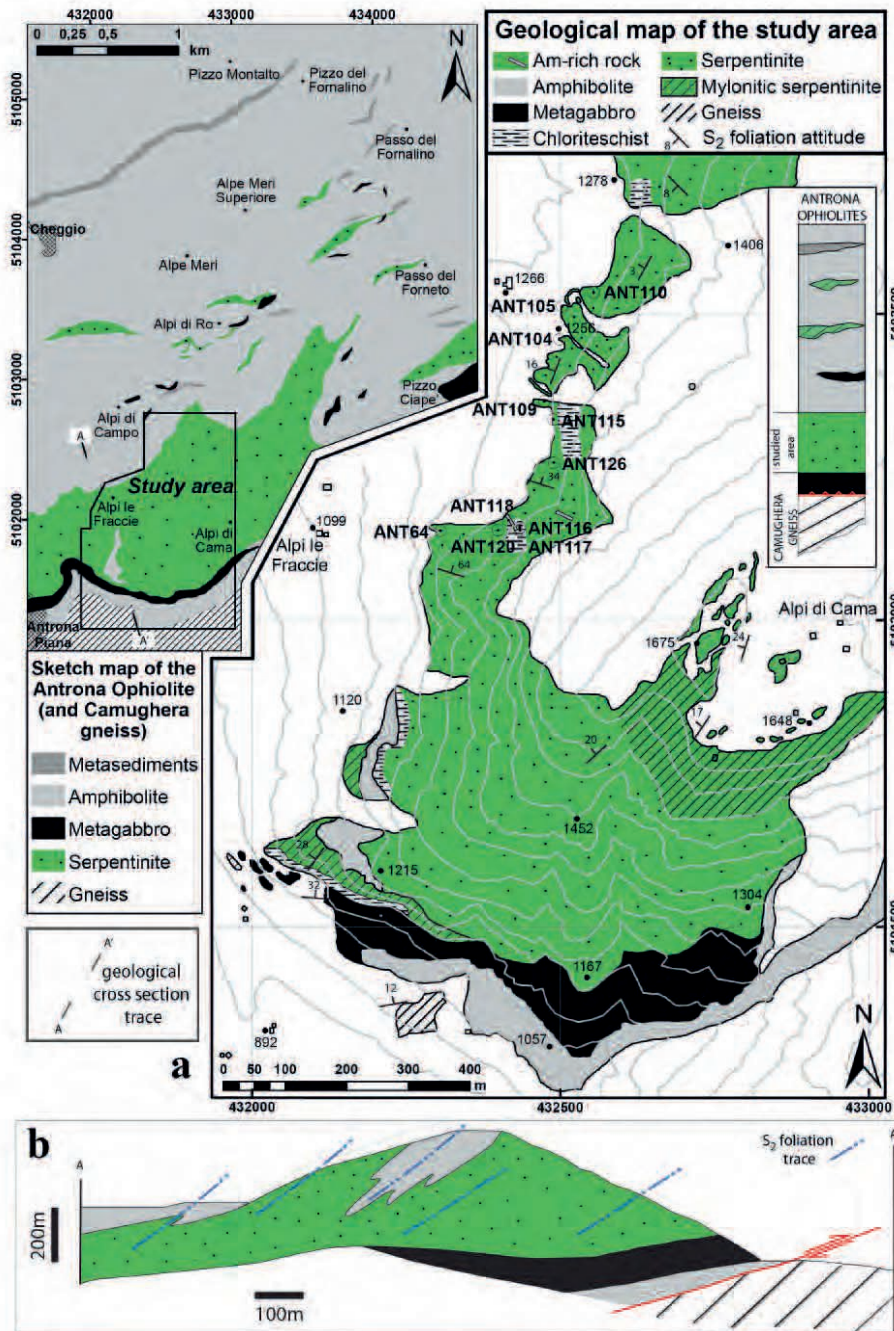


Fig. 2 - Geology of the study area. a) Geological map of the Antrona ophiolite with location of the study area (inset). b) Detailed geological map of the study area and synthetic lithostratigraphy log reconstructed by single outcrops. Location of the collected samples (e.g., ANT110) is also shown. c) Schematic cross section along the AA' trace shown Fig. 2b.

mation generating crenulation of the S_2 foliation or chevron folds (Table 1; see also Fig. 6b), commonly concentrated near the contact between serpentinites and harder mafic rocks. D_3 folds do not develop axial plane foliation visible at the outcrop scale but concur to the high dispersion of S_2 data (Table 1).

D_4 phase

Late S-C type structures and fractures (D_4) overprint all previous structures, commonly generating lozenge-shaped rock volumes at all scales (Table 1).

Microstructural analysis

Thin-section investigations were addressed to characterize the composition and microstructure of the ultramafic rocks. Sample location is shown in Fig. 2. A complete list

of the investigated samples and their qualitative modal composition are reported in Table 2. Our observations reveal that most samples are characterized by a pervasive foliation corresponding to the regional schistosity recognized in the field (S_2), which is commonly marked by phyllosilicate minerals, such as serpentine and chlorite. Moreover, the microstructural analysis allowed recognizing structures that are not always detectable in the field, including either relict structures that predate the S_2 foliation or late foliations superimposed to S_2 .

A synthetic scheme of the microstructural evolution relative to mineral growth of the studied rocks is reported in Table 3. In the following description, subscripts refer to the relative timing of mineral growth while subscripts "p" and "n" refer to microstructural characters and specifically, porphyroblasts and neoblasts, respectively. Mineral abbreviations according to Siivola and Schmid (2007).

Table 1 - Synthesis of the mesostructural analysis of the studied rocks.

PHASE	SERPENTINITE		STRUCTURE ORIENTATION
D1+D2	a) D2 folding of S1 pre-S1 structure	b) Lozenge-shaped mineral aggregate	S2 foliation
	c) D2 folding of S1	d) amph-layer chloriteschist	
D3	magnetite D3 crenulation of S2 foliation		D3 axes and axial planes
D4	D4 fractures		D4 structures

D- deformation phase; S- foliation. Structure orientations are plotted in equal area Schmidt stereographic projections, lower hemisphere.

Table 2 - List of the studied samples with GPS coordinates and qualitative modal composition.

Sample	X	Y	Rock type	Minerals (with relative modal abundance)
ANT 104	432498	5102459	foliated serpentinite	srp55%, ol35%, mag5%, cpx5%
ANT105	432503	5102513	Amp-chloriteschist	chl40%(including pseud. after cpx), amp25%, cb25%
ANT108	431978	5101595	Amp-chloriteschist	chl54%, amp 45%, ep+tnt 1%
ANT109	432474	5102358	foliated serpentinite	srp30%, chl25%, amp35, cpx10%
ANT110	432554	5102535	cpx-rich layer	cpx90%, chl5%, opaque2%
ANT111	432554	5102531	cpx-rich layer	cpx70%, mag25-30%
ANT112	432951	5102872	chloriteschist	chl90%, opaque5%-10%
ANT114	432588	5102599	chloriteschist	chl85%, mag15%
ANT115	432489	5102328	foliated serpentinite	srp50%, ol20%, mag15%, chl10, cpx5%
ANT116	432434	5102152	chloriteschists	chl65%, amp35%, opaque2%
ANT117	432435	5102147	chloriteschist	chl30%, amp10%, chl+amp (groundmass)60%
ANT118	432415	5102164	amp-rich layer	amp80%, pl20%, tnt
ANT119	432399	5102148	amp-cpx-chl-rock	amp50%, cpx30%, mag10%, chl5%, tlc5%, ol
ANT120	432399	5102147	ol-cpx-amp-rock	ol40%, amp30-35%, chl20%, mag5% (cpx)
ANT121	432449	5102183	amp-cpx-chl-rock	amp65%, cpx20%mag10%, chl5%, (ol)
ANT124	432768	5101953	serpentinite	srp70%, cb15-20%, mag10%, opaque
ANT126	432490	5102258	amp-chl-rock	amp45%, mag+chl20% cpx+ol 35%
ANT128	432788	5102019	chloriteschist	chl55%, amp40%, mag5%
ANT129	432464	5102237	chloriteschist	chl85-90%, amp10-15%, opaque2%
ANT131	432754	5101889	serpentinite	srp80-85%, mag15%, opaque5%
ANT132	432597	5102620	cpx-rich layer	cpx55%, chl30%, mag+chl15%
ANT133	432757	5101908	serpentinite	srp50%, cb20%mag10%, amp (replacing cpx)20%
ANT64	432306	5102147	dunite	ol90%, spl+chl10%, spl, srp

In bold: samples mentioned in the text.

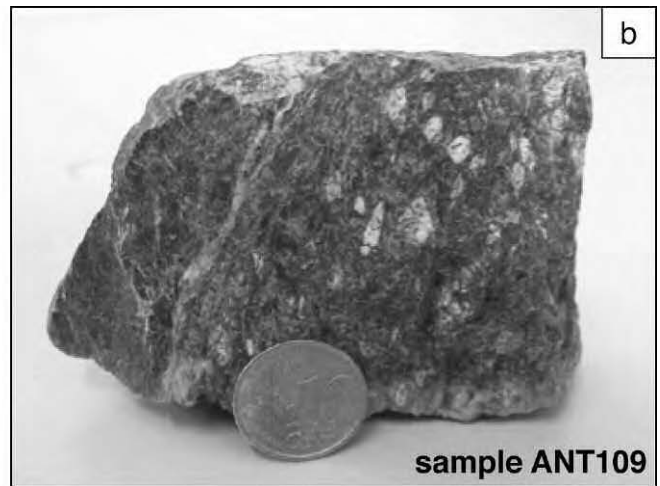
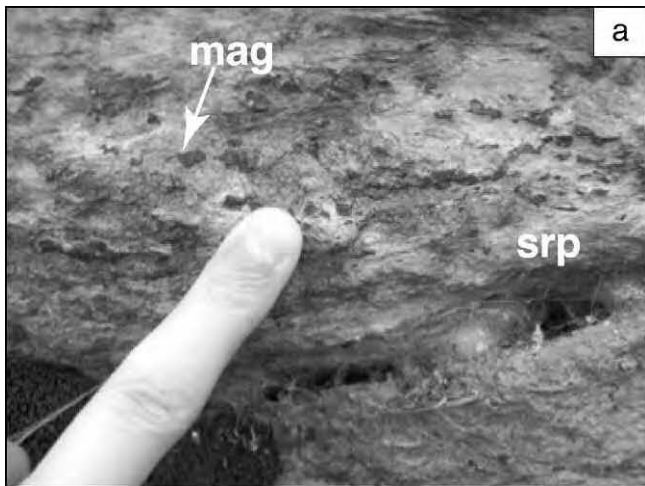


Fig. 3 - Field occurrences: a) Serpentinite with magnetite grains and fine-grained aggregates elongated parallel to the rock foliation. b) Serpentinite sample showing millimetric, lozenge-shaped, whitish mineral aggregates consisting of clinopyroxene+amphibole \pm chlorite+magnetite.

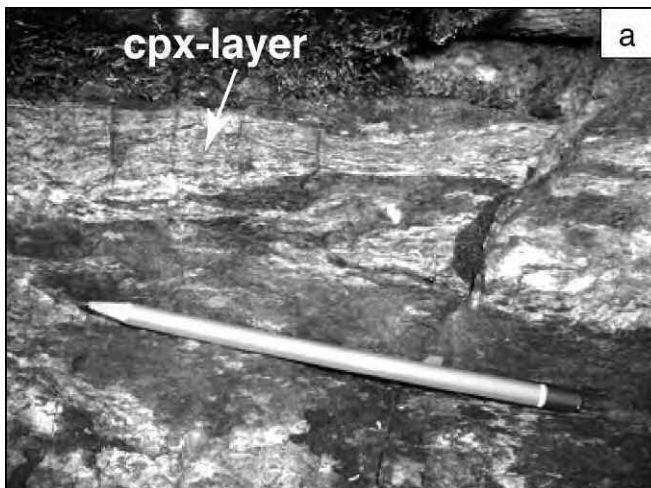


Fig. 4 - Field occurrences: a) Centimetric white-to-greenish layers ("cpx-rich layer") transposed within the serpentinite foliation. b) Amphibole-rich rocks included in serpentinite.

Several structures in serpentinites and less serpentinized ultramafic rocks can be interpreted as being older than the main penetrative foliation S_2 , and then attributed to early stages of the Alpine evolution or earlier; they are pre- S_1 structures and the S_1 relict foliation. As a consequence, the S_2 foliation constitutes a fundamental reference point in the structural reconstruction.

Pre- S_1 structures

In serpentinites, we often observed lens-shaped or rectangular pseudomorphous sites of serpentine, probably replacing an earlier igneous mineral (pyroxene?; Fig. 5a; Table 3a). In less serpentinized ultramafic rocks, fresh olivine, clinopyroxene, spinel, and minor magnetite are still preserved. In less foliated samples, olivine is present as round-shaped and fractured millimetric porphyroblasts characterized by a porphyroblastic texture. Olivine porphyroblasts (Ol_p ; Table 3a) commonly show intracrystalline deformation attested by the presence of wavy extinction and subgrain boundaries (or "kink-bands" = KB; Mercier and Nicolas 1975; Fig. 5b, c). Dunite layers and pods (e.g., sample ANT64) consist of olivine, spinel, opaque minerals, chlorite, \pm serpentine and preserve the pre- S_1 microstructure. This rock is very fine-

grained, so no clear foliation is visible in the field. Nevertheless, dunites reveal, under the microscope, the occurrence of a well defined foliation ("pre- S_1 "; Fig. 5d), marked by the shape-preferred orientation (SPO) of olivine. Olivine is present as coarse-grained (mm- to cm-sized) porphyroblasts (Ol_p), commonly elongated and strained. Intracrystalline deformation is attested by the presence of kink-bands ("KB" in Fig. 5d). The angle between foliation and kink-bands boundaries (KBB) is about 45° .

Among less altered foliated serpentinites, coarse-grained ol \pm cpx \pm spl (\pm am, \pm chl)-rich rocks (e.g., sample ANT120; Table 3d) are characterized by mm-sized olivine porphyroblasts showing intracrystalline deformation and olivine neoblasts (Fig. 5e), relict clinopyroxene porphyroclasts, and mm-scale chl + am pseudomorphs (replacing orthopyroxene?) (Fig. 5f; Table 3d). Spinel crystals are sub-millimetric and their shape recalls the holly-leaf habit described in mantle-derived peridotites (e.g., Mercier and Nicolas 1975; Nicolas and Poirier 1976; Fig. 5g). Spinel is always rimmed by a thick corona made of chlorite (Fig. 5g). Spinel with a similar shape was observed also in dunite sample (ANT64; Fig. 5h). The coarse-grained ol \pm cpx \pm spl-rich rocks are recrystallized

Table 3 - Synthesis of the microstructural analysis of the studied rocks.

a) SERPENTINITE				
	pre-S1	S1	S2	post-S2
Srp _p	█	█ █ █		
Srp			█ █ █ █ █	█ █ █ █ █
Srp-v				█ █ █ █ █
Ol _p	█			
Ol _n		█ █ █ █ █		
Cpx _p	█			
Cpx _n		█ █ █ █ █		
Spl	█ █ █ █ █			
Cr-Chl+FeChr	█ █ █ █ █	█ █ █ █ █	█ █ █ █ █	
Mag		█ █ █ █ █	█ █ █ █ █	
Cpx+Am, Chl, Mag aggregate		█ █ █ █ █	█ █ █ █ █	
Cal				█ █ █ █ █

d) COARSE-GRAINED OL-RICH ROCK				
	pre-S1	(S1)	S2	post-S2
Ol _p	█			
Ol _n		█ █ █ █ █		
Cpx _p	█			
Cpx _n		█ █ █ █ █		
Spl	█ █ █ █ █			
Chl-Am aggregate		█ █ █ █ █	█ █ █ █ █	
Chl _c		█ █ █ █ █	█ █ █ █ █	

b) Cpx-rich LAYERS				
	pre-S1	S1	S2	post-S2
Cpx _p	█ █ █ █ █			
Di _p		█ █ █ █ █	█ █ █ █ █	
Di _n			█ █ █ █ █	
Chl			█ █ █ █ █	█ █ █ █ █
Mag		█ █ █ █ █	█ █ █ █ █	

c) CHLORITESCHIST				
	pre-S1	(S1)	S2	incipient S3
Chl			█ █ █ █ █	█ █ █ █ █
Am			█ █ █ █ █	█ █ █ █ █
Mag		█ █ █ █ █	█ █ █ █ █	

e) DUNITE				
	pre-S1	(S1)	S2	post-S2
Ol _p	█			
Ol _n		█ █ █ █ █		
Srp		█ █ █ █ █	█ █ █ █ █	█ █ █ █ █
Spl	█ █ █ █ █			
Cr-Chl		█ █ █ █ █	█ █ █ █ █	

f) Am-RICH LAYER				
	pre-S1	S1	S2	post-S2
Am			█ █ █ █ █	█ █ █ █ █
Pl			█ █ █ █ █	
Ttn			█ █ █ █ █	
Chl _p		█ █ █ █ █	█ █ █ █ █	█ █ █ █ █

Number refers to the relative timing of mineral growth while subscripts "p" and "n" refer to microstructural characters and specifically, porphyroblasts and neoblasts, respectively. Minerals abbreviations according to Siivola and Schmid R. (2007).

at various extents into am + chl-rich rocks (e.g., samples ANT119, ANT121, ANT126; see Table 2); the resulting mineral assemblage and foliation thus depend on the extent of rock recrystallization.

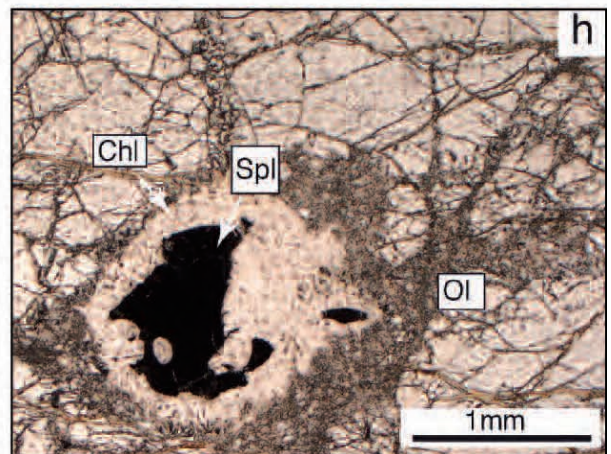
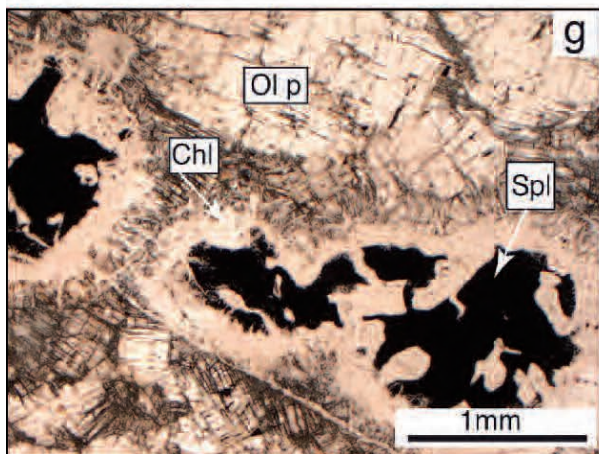
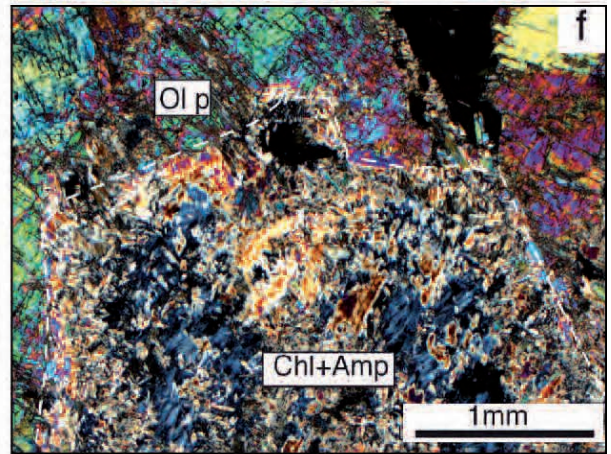
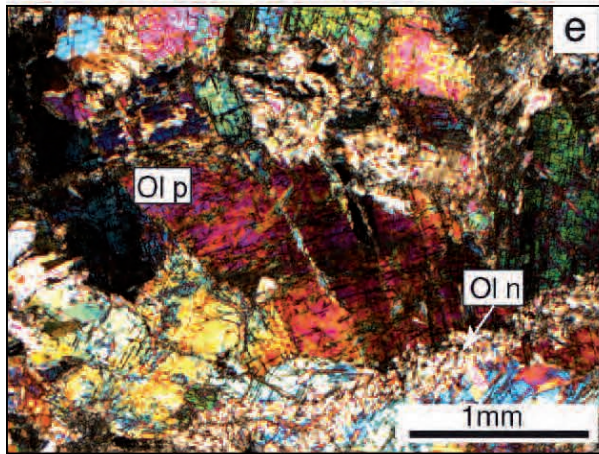
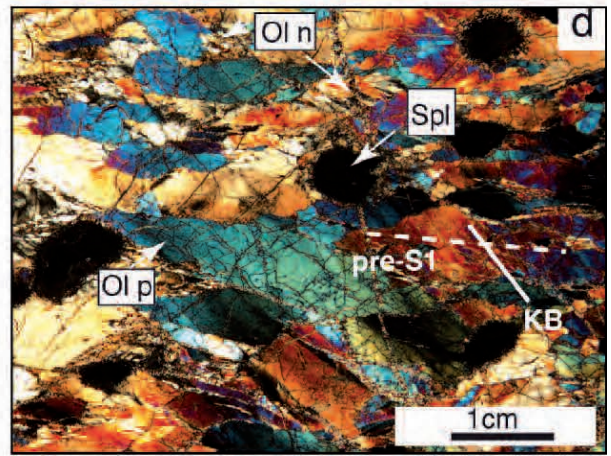
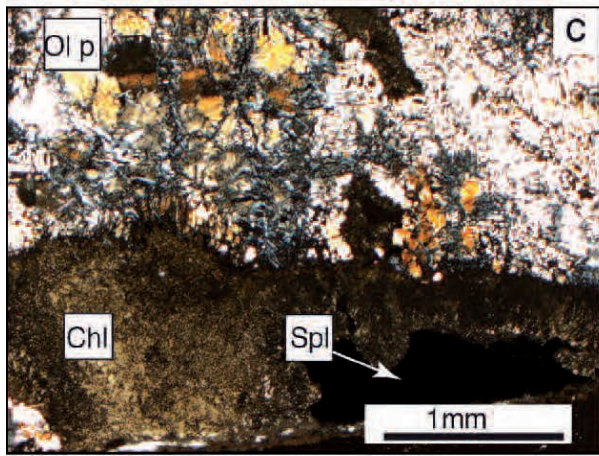
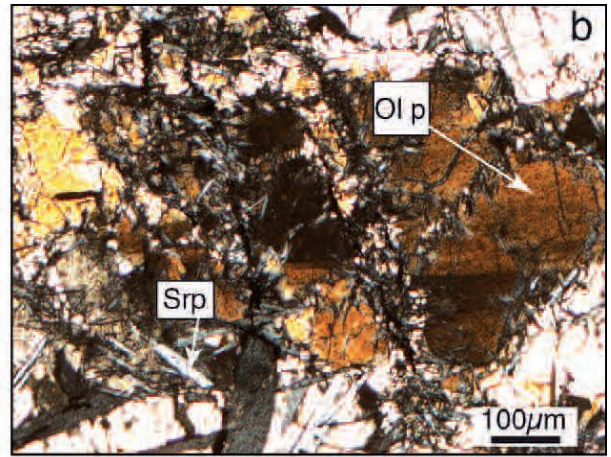
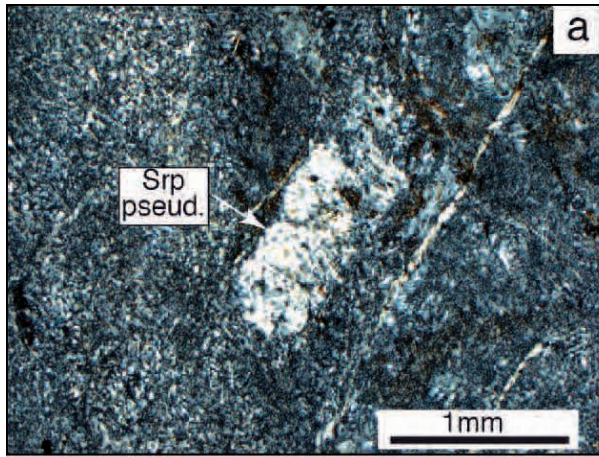
S₁ foliation

In some samples, Ol_p and clinopyroxene porphyroblasts (Cpx_p) are rimmed by fine-grained neoblastic olivine (Ol_n) and clinopyroxene (Cpx_n), respectively. In more recrystallized samples or sample portions, Ol_p and Cpx_p are almost completely replaced by neoblastic grains forming polycrystalline layers (S₁) infolded within the S₂ foliation (Fig. 6a, b). These layers correspond to the millimetric, brownish ol + cpx-layers recognized in the field (see Table 1a).

In less foliated samples, clinopyroxene porphyroblasts (Cpx_p) contain coarse exsolution lamellae often filled with

opaque minerals (Fig. 6c). In more recrystallized rocks, clinopyroxene neoblasts (Cpx_n) rim clinopyroxene porphyroblasts (Cpx_p) and more commonly occur in mineral aggregates together with Ol_n grains and opaque minerals, defining the S₁ foliation. Clinopyroxene neoblasts have also crystallized along bands of kinked Cpx_p (bulging-BLG-recrystallization? See Fig. 7b). Spinel is anhedral and opaque in thin section. It is almost always rimmed by chlorite (see Fig. 5c). Magnetite occurs as 2-3 μm sized anhedral grains or grain aggregates (e.g., in sample ANT104).

Olivine neoblasts (Ol_n) in dunites grow at the rim of Ol_p but more often they fill intercrystalline fractures in association with serpentine crystals (Ol_n; see Fig. 5d and Table 3e). Spinel occurs as mm-sized holly-leaf shaped crystals or ovoidal porphyroblasts mantled by a chlorite rim (see Fig. 5e).



Summing up, the porphyroblastic mineral assemblage of olivine, clinopyroxene, and spinel (Ol_p , Cpx_p , Spl) in foliated serpentinites and olivine and spinel porphyroblasts in dunites can be attributed to an early, pre- S_1 (mantle-derived?) stage (see Discussion), followed by the S_1 development marked by the oriented neoblastic growth of olivine and clinopyroxene (e.g., Ol_n and Cpx_n).

Other relict pre- S_2 structures were recognized inside the centimetric white-to-greenish layers observed in the field (e.g., sample ANT110, see Fig. 4a and Table 1c) showing a composition ranging from clinopyroxenite to clinopyroxene-bearing chloriteschists. In such rocks, clinopyroxene shows three different textures (Table 3b): relict porphyroblast (Cpx_p) containing exsolution lamellae often filled with opaque minerals (see Fig. 6d, e), mm-sized diopside porphyroblasts (Di_p), often arranged in fan-shaped aggregates showing wavy extinction (Fig. 6e, f), and fine-grained granoblastic-neoblastic diopside (Di_n), sometimes showing polygonal or mosaic-texture (Fig. 6d, e, f). Porphyroclastic Cpx_p and porphyroblastic Di_p are here interpreted as relict pre- S_2 structures (Table 3b).

Main penetrative S_2 foliation

Pervasive S_2 foliation is defined in most rocks by serpentine. In foliated (eg., samples ANT104, ANT105, ANT109, ANT115) and mylonitic serpentinites, serpentine (Srp) forms fine-grained crystals aligned along S_2 (Table 3a). In some foliated serpentinites, S_2 is marked by millimetric boudins or lozenge-shaped aggregates of fine-grained $cpx + am \pm chl + mag$ (Fig. 6g; see also Fig. 3b, Table 1b, and Table 3a). These lenses or boudins are interpreted as deriving by replacement of earlier clinopyroxene, since relict clinopyroxene porphyroclasts are still locally recognizable (Fig. 6h). Consequently, the lozenge-shaped aggregates, although now oriented parallel to S_2 structures, may represent relict pre- S_2 structures.

Mylonitic serpentinites are made of serpentine, magnetite, and carbonate. No relict olivine, pyroxene, and spinel were recognized, except for the occurrence of pseudomorphic aggregates of fine-grained serpentine filling sub-rounded or rhombic pseudomorphic sites. Serpentine crystals with SPO mark the mylonitic S_2 foliation often deformed by small-scale D_3 crenulation. Ca-carbonate occurs as millimetric porphyroblasts showing intracrystalline deformation as well as smaller grains distributed in the serpentine groundmass.

In the cpx -rich layers transposed within the serpentinites (see Fig. 4a), the S_2 foliation is defined by fine-grained granoblastic-neoblastic clinopyroxene (Di_n), sometimes with polygonal or mosaic-texture (see Fig. 6d, e, f; Table 3b).

In chloriteschists (e.g., samples ANT116, ANT117, ANT108; Table 2) the S_2 foliation is defined by chlorite and amphibole crystals and is superimposed by incipient S_3 foliation (Table 3c).

The amphibole-rich layers (e.g., sample ANT118; Table 2) consist of fine-grained aggregates of amphibole (~80%) and minor plagioclase and sphene oriented parallel to the S_2 foliation. Few sub-millimetric anhedral crystals of amphibole or chlorite (pseudomorphs?) were observed in the fine-grained groundmass (Table 3f).

In coarse-grained Ol -rich rocks (e.g., sample ANT120) and in dunites (e.g., sample ANT64) the S_2 foliation is not visible and the static growth of $chl \pm am \pm srp$ is the only microstructure likely related to D_2 stage.

Post- S_2 structures

Post- S_2 structures are represented by coarse-grained acicular crystals of serpentine or amphibole, which define an incipient and discontinuous S_3 foliation, superimposed to the main foliation S_2 , and by veins. Veins are widespread in serpentinites and chloriteschists and are commonly filled with serpentine or chlorite fibres. All vein types crosscut all other structures, and are then later than pervasive S_2 and incipient S_3 foliations (Table 3).

MINERAL CHEMISTRY

Microchemical analyses were performed with WDS-X-Ray spectrometer system connected to JEOL 8200 Super Probe at the Electron Microprobe Laboratory of the Università degli Studi di Milano, Dipartimento di Scienze della Terra. These quantitative analyses were carried out at 15 kV accelerating voltage and 15 nA beam current with a spot size of 1 μm . The counting time was 30s for peak and 10s for backgrounds. A series of natural minerals and pure metals were used as standards. The matrix corrections were calculated with the ZAF procedure. Mineral formulas have been recalculated using Recalc3, Norms2, AmphIMA97. Fe^{2+}/Fe^{3+} repartition was performed according to Droop (1987). Selected analyses are reported in Tables 4-9. Chemical compositions discussed in the following are related to the all analyses here performed. Rock type and mineralogy and relative modal abundance are summarised in Table 2 for all cited samples.

Clinopyroxene

Clinopyroxene was analyzed only in foliated serpentinites (sample ANT104). The chemical composition of clinopyroxene is very close to the diopside end member (Table 4). However, recrystallization of clinopyroxene porphyroblast (Cpx_p) into clinopyroxene neoblasts (Cpx_n) is accompanied by a decreasing in Al and increasing in Ca contents (Table 4; analyses 104-3-6 and 104-3-8, respectively; see also Fig. 7). Back-scattered electron (BSE) images reveal the complex texture of relict clinopyroxene

Fig. 5 - Photomicrographs of representative samples: pre- S_1 structures. Mineral abbreviations according to Siivola and Schmid (2007). a) Rectangular serpentine pseudomorph (after previous pyroxene?) in serpentinite (sample ANT109). Crossed nicols. b) Olivine porphyroblast (Ol_p) with intracrystalline deformation attested by the presence of subgrains ("deformation lamellae") in partially serpentinized peridotite (sample ANT115). Crossed nicols. c) Olivine porphyroblast (Ol_p) with internal kink-bands and anhedral spinel (Spl) rimmed by chlorite (sample ANT115). Crossed nicols. d) Elongate, coarse-grained olivine porphyroblasts (Ol_p) showing intracrystalline deformation, and smaller neoblasts grains (Ol_n) in fresh dunite (sample ANT64). Olivine shape preferred orientation almost coincides with rock foliation (pre- S_1) which describes an angle of about 45° with kink-bands boundaries (KB). Crossed nicols. e) Coarse-grained olivine porphyroblast (Ol_p) showing intracrystalline deformation, and olivine neoblasts (Ol_n) in olivine-clinopyroxene-spinel-rich rocks (sample ANT120). Crossed nicols. f) Coarse-grained olivine and mm-scale chlorite+amphibole pseudomorphs (replacing orthopyroxene?) (sample ANT120). Crossed nicols. g) Coarse-grained spinel crystal with a holly-leaf habit, rimmed by chlorite (sample ANT 120). Plane-polarised light. h) Ovoidal spinel porphyroblast mantled by a chlorite rim and coarse-grained olivine in dunite (sample ANT64).

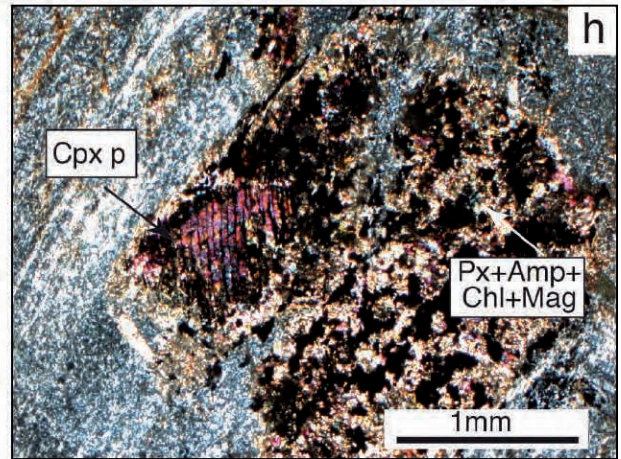
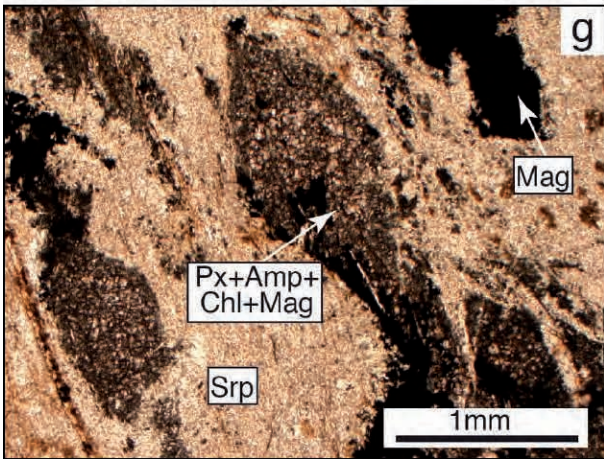
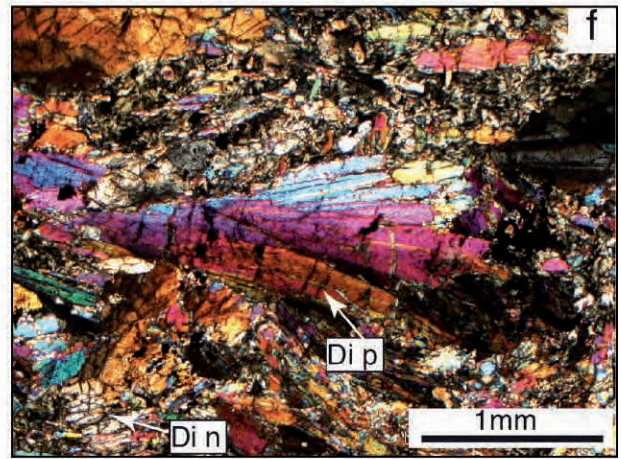
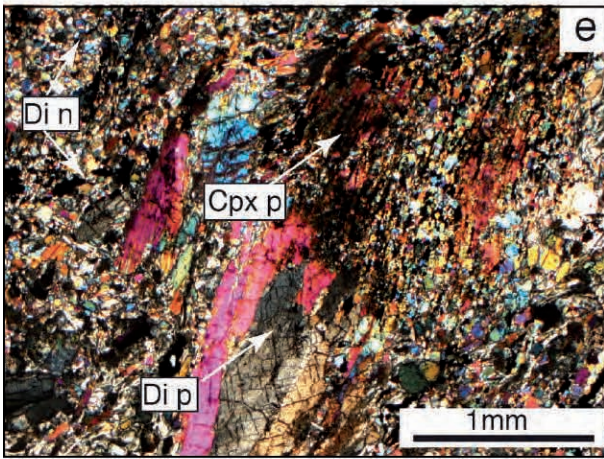
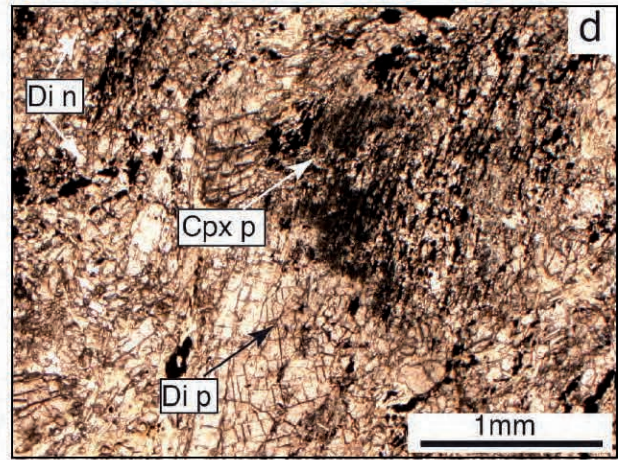
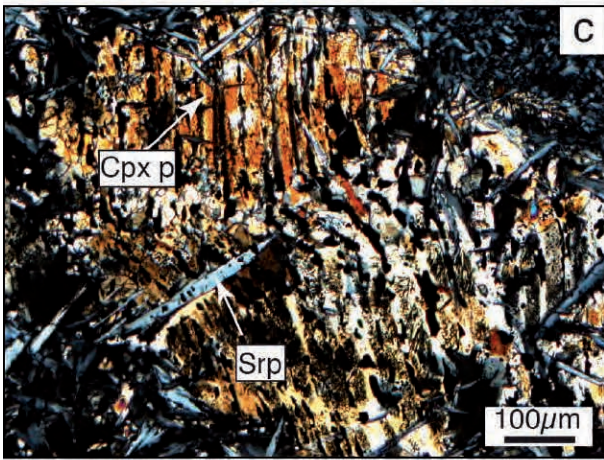
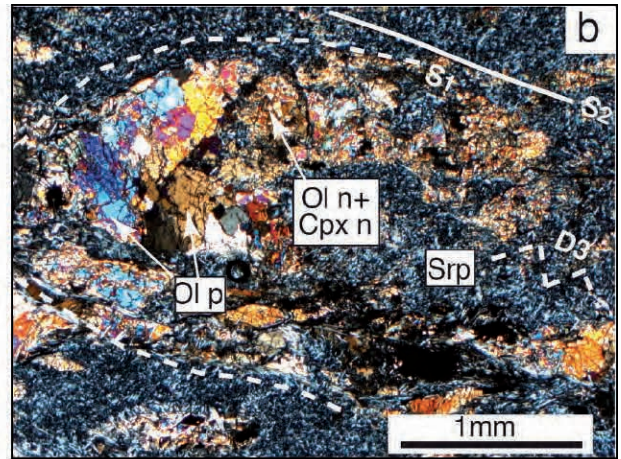
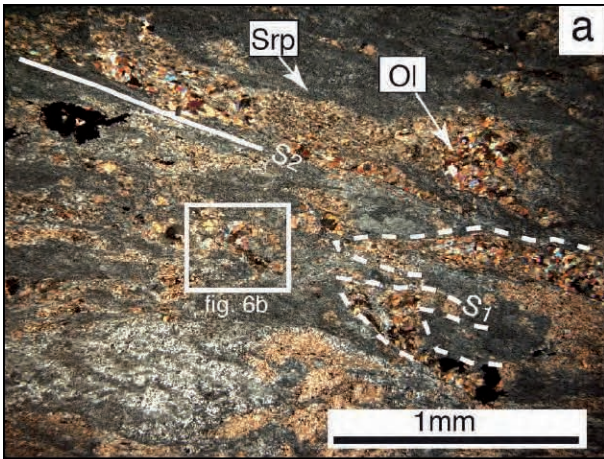


Table 4 - Representative microchemical composition of clinopyroxene.

Sample	ANT104	ANT104	ANT104	ANT104	ANT104
Rock type	foliated S.				
Analysis #	104-2-22	104-3-6	104-3-8	104-5-15	104-6-17
Texture	Cpx n	Cpx p	Cpx n	Cpx n	Cpx n
wt%					
SiO ₂	56.26	53.46	56.37	56.27	56.27
TiO ₂	bdl	0.16	bdl	0.06	bdl
Al ₂ O ₃	bdl	3.06	bdl	bdl	bdl
Cr ₂ O ₃	0.04	0.83	bdl	bdl	0.04
FeO	1.17	1.66	1.34	0.96	1.1
MnO	0.04	0.06	0.05	bdl	0.03
MgO	18.14	16.57	18.07	18.08	17.94
CaO	26.02	24.9	26.04	26.2	26.1
Na ₂ O	bdl	0.2	bdl	bdl	bdl
Ox Total	101.67	100.9	101.87	101.57	101.48
Normalization on the basis of 4 CATIONS					
Si	2.002	1.913	2.004	2.004	2.006
Ti	-	0.004	-	0.002	-
Al IV	-	0.087	-	-	-
Al VI	-	0.042	-	-	-
Cr	0.001	0.023	-	-	0.001
Fe ₃	0.000	0.027	0.000	0.000	0.000
Fe ₂	0.035	0.050	0.040	0.029	0.033
Mn	0.001	0.002	0.002	0.001	0.001
Mg	0.962	0.884	0.957	0.960	0.954
Ca	0.992	0.955	0.992	1.000	0.997
Na	-	0.014	-	-	-
Cat Total	3.993	4.001	3.995	3.996	3.992
Wo	49.87	50.55	49.86	50.28	50.27
En	48.38	46.81	48.14	48.28	48.08
Fs	1.75	2.64	2	1.45	1.65
Sum	100	100	100	100	100

Cpx p and Cpx n are clinopyroxene porphyroblasts and neoblasts, respectively.

porphyroblasts (Cpx_p) that are often deformed by kinking and replaced by various mineral phases (Fig. 7a, b). Magnetite grows along exsolution lamellae (probable former orthopyroxene, although fresh orthopyroxene was not found in the analyzed samples) inside Cpx_p (Fig. 7b; see Table 5 for magnetite composition). New clinopyroxene grains have crystallized at the expense of Cpx_p and also along bands of kinked Cpx_p (Fig. 7b); finally, late amphibole (tremolite; see analysis 104-3-4 in Table 8) and serpentine crystals statically grow on Cpx_p.

Olivine

Olivine was analyzed in serpentinites (samples ANT104, ANT120) and dunites (sample ANT64). Olivine composition ranges between Fo₈₇ and Fo₈₈ in samples ANT104 and ANT120, while in dunite ANT64 olivine has higher Mg contents (Fo₉₀). In all samples, olivine neoblasts and porphyroblasts have comparable compositions (Table 5). Different compositions of olivine from serpentinites and dunites may be related to the original bulk rock compositions.

Fig. 6 - Photomicrographs of representative samples: S₁ and later structures. Mineral abbreviations according to Siivola and Schmid (2007). a) Polycrystalline S₁ layers of olivine ± clinopyroxene infolded within S₂ foliation in a partially serpentinized peridotite (sample ANT104). Crossed nicols. The inset shows the location of picture 6b. b) Detail of Fig. 6a) showing olivine porphyroblasts (Ol p) and neoblasts (Ol n) near the fold hinge of S₁ layer infolded in the S₂ foliation (sample ANT104). The Ol-Cpx layer is also crenulated by D₃ deformation phase (D3). Crossed nicols. c) Relict clinopyroxene porphyroblast (Cpx p) containing exsolution lamellae filled with opaque minerals (sample ANT104). Crossed nicols. d) Relict clinopyroxene porphyroblast (Cpx p) containing exsolution lamellae filled with opaque minerals in clinopyroxenite layer (sample ANT110). Diopside porphyroblasts (Di p) and neoblasts (Di n) are also shown. Plane polarized light. e) Same as Fig. 6a but under crossed polarized light. f) Millimetric-scale clinopyroxene (diopside) porphyroblast (Di p) arranged in fan-shaped aggregates with wavy extinction (sample ANT110). Crossed nicols. g) Layers and boudins made of fine-grained clinopyroxene+amphibole ± chlorite+magnetite, transposed within S₂ foliation (sample ANT109). Plane polarized light. h) Relict clinopyroxene porphyroblast (Cpx p) recrystallized into aggregates of fine-grained pyroxene + amphibole + chlorite + magnetite (sample ANT109). Crossed nicols.

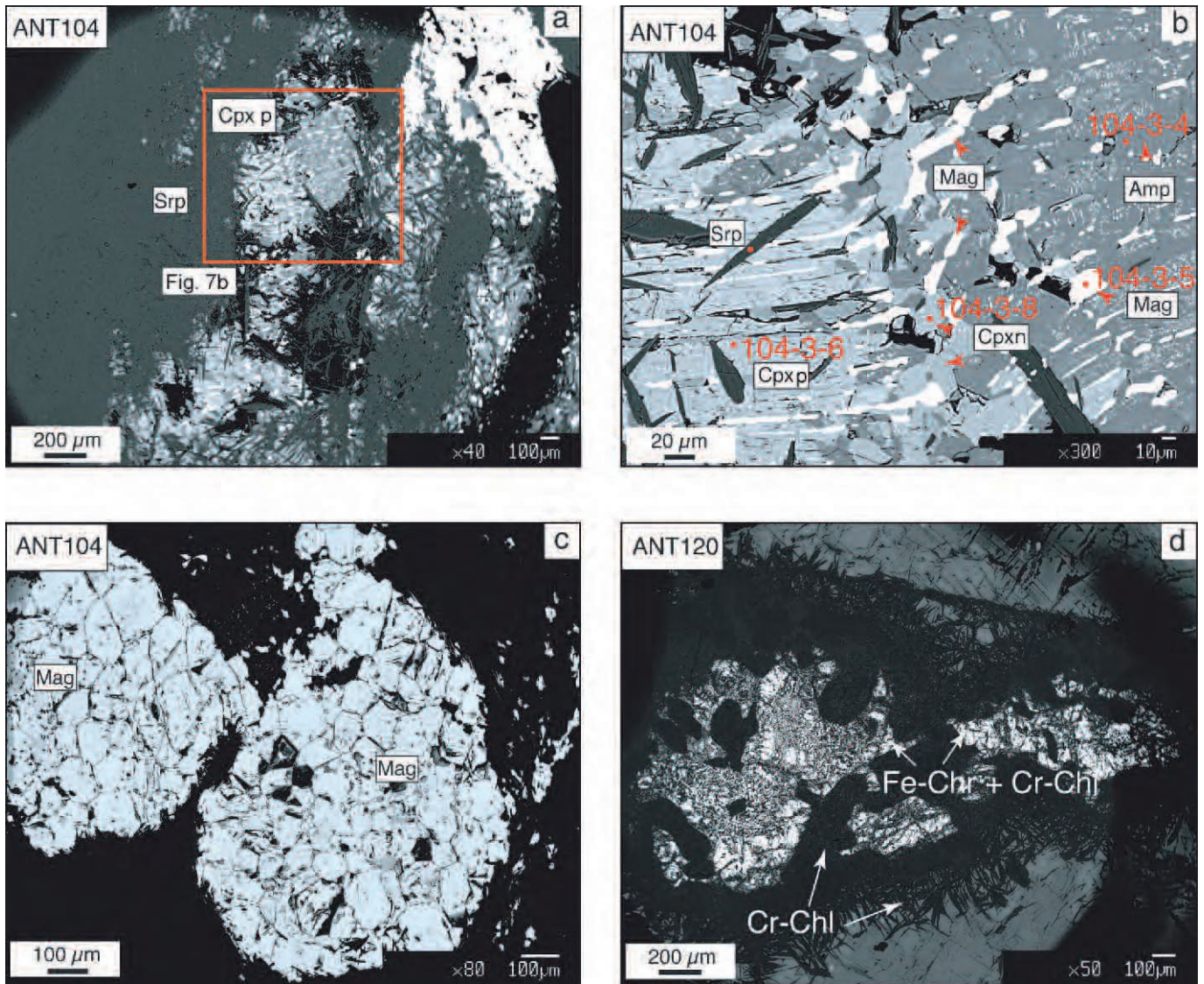


Fig. 7 - Back Scattered Electron-SEM images of the analyzed samples. Mineral abbreviations according to Siivola and Schmid (2007). a) Cpx porphyroblast deformed by kinking. b) Detail of Fig. 7a. Analyzed spots and relative analysis labels as reported in Table 4 are also shown. c) Polycrystalline aggregates of magnetite with mosaic texture. d) Ferritchromite crystal with porous texture, rimmed by Cr-chlorite.

Spinel

Two main compositions were found among the analyzed spinel: magnetite and chromite (Table 6). Magnetite occurs as polycrystalline aggregates with mosaic texture (Fig. 7c) in serpentinized peridotites (sample ANT104; Table 6). Cr-rich spinel occurs in coarse-grained ol-cpx-spl (\pm am, \pm chl)-rich rocks (sample ANT120), where it shows holly leaf-shaped morphology and is commonly mantled by chlorite (see Fig. 5g). BSE images of such spinel crystals reveal a porous texture without any evident core-to-rim zoning (Fig. 7d). These crystals have a ferritchromite composition with $100[\text{Cr}/(\text{Cr} + \text{Al})]$ atomic ratios ranging between 96 and 98. Cr_2O_3 ranges between 53 and 58 wt%; MgO between 1.7 and 1.9 wt%; Al_2O_3 between 0.7 and 0.8 wt%; FeOt wt% ranges between 35 and 40. In dunite ANT64, Cr_2O_3 ranges between 55 and 58 wt%; MgO between 2.4 and 3.2 wt%; Al_2O_3 between 1 and 1.4 wt%; and FeOt wt% ranges between 35 and 37. Thus also in dunites, spinel has a ferritchromite composition; $100[\text{Cr}/(\text{Cr} + \text{Al})]$ atomic ratios ranges between 96 and 97.

Serpentine

The composition of natural serpentine has generally small deviance from the ideal formula: $\text{Mg}_3[\text{Si}_2\text{O}_5](\text{OH})_4$ (Wicks and O'Hanley, 1988). Substitution is mainly performed by Al both in tetrahedral and octahedral site (i.e., tschermak substitution). These substitutions imply a solid solution and/or interstratification among serpentine, chlorite and amesite (i.e., septechlorite; Nelson and Roy, 1958; Chernosky et al., 1988; Bailey 1988a; 1988b; Bailey et al., 1995). Serpentine was analyzed in serpentinites (sample ANT104), where it shows three main textures: fine-grained crystals in the groundmass, acicular crystals overgrowing the groundmass, and fibrous crystals filling veins. In general, all the analyzed serpentine crystals have relatively high Al_2O_3 contents suggesting that they are rich in the amesite components. However, serpentine in veins is characterized by lower Al_2O_3 contents relative to serpentine in all other textures (Table 7).

Table 5 - Representative microchemical composition of olivine.

SAMPLE	ANT120	ANT120	ANT64	ANT64	ANT104	ANT104
Rock type	ol-cpx-am-S	ol-cpx-am-S	dunite	dunite	foliated S.	foliated S.
Analysis #	C-1	C-12	B-13	B-14	C-19	B-9
Texture	Ol1	Ol1	Ol _p	Ol _n	Ol _p	Ol _n
wt%						
TiO ₂	bdl	bdl	0.04	bdl	bdl	bdl
SiO ₂	40.38	40.14	41.06	40.98	40.56	40.25
Al ₂ O ₃	bdl	bdl	bdl	bdl	bdl	bdl
Cr ₂ O ₃	bdl	0.07	bdl	bdl	bdl	bdl
FeO	11.70	11.60	9.72	9.72	11.83	11.94
MnO	0.24	0.26	0.18	0.17	0.33	0.33
MgO	46.88	47.50	49.41	49.29	46.67	46.76
ZnO	bdl	bdl	bdl	bdl	bdl	bdl
CaO	bdl	bdl	bdl	bdl	bdl	bdl
K ₂ O	bdl	bdl	bdl	bdl	bdl	0.02
NiO	0.42	0.43	0.45	0.33	0.43	0.38
Ox Total	99.67	100.07	100.87	100.51	99.86	99.69
Normalization on the basis of 4 OXYGENS (no Fe ³⁺)						
Ti	-	-	0.001	-	-	-
Si	1.003	0.994	0.998	0.999	1.006	1.001
Al	-	-	-	-	-	0.000
Cr	-	0.001	-	-	-	0.000
Fe ₂	0.243	0.240	0.198	0.198	0.245	0.248
Mn	0.005	0.006	0.004	0.003	0.007	0.007
Mg	1.736	1.754	1.791	1.792	1.726	1.734
Zn	-	-	-	-	-	-
Ca	-	-	-	-	-	-
K	-	-	-	-	-	0.001
Ni	0.008	0.009	0.009	0.006	0.009	0.008
Cat Total	2.996	3.004	3.000	3.000	2.993	2.998
recalc Fe ³⁺	0.000	0.011	0.000	0.000	0.000	0.000
ENDMEMBERS						
Forsterite	87	87.7	89.9	90	87.2	87
Fayalite	12	12.0	9.9	10	12.4	12
Tephroite	0	0.3	0.2	0	0.4	0

Ol1- coarse-grained olivine porphyroblasts in sample ANT120; Ol_p and Ol_n- olivine porphyroblasts and neoblasts, respectively, in dunite ANT64 and sample ANT104.

Amphibole

All amphibole crystals analyzed in serpentinite samples (ANT104 and ANT120) are tremolite (according to Leake et al. 1997's nomenclature; Table 8). These include: amphibole replacing clinopyroxene porphyroblasts (see Fig. 7b; analysis 104-3-4 in Table 8) and late acicular amphibole crystals in serpentinite ANT104, as well as amphibole replacing olivine and amphibole in chl + am pseudomorphs in sample ANT120 (see Fig. 5f).

Chlorite

Chlorite was analyzed in samples ANT120 and ANT64, where it surrounds holly-leaf-shaped ferritchromite (see Fig. 5g, h). BSE images show that chlorite occurs not only as acicular crystals in coronae surrounding spinel but also as crystals intimately associated with porous ferritchromite core (Fig. 7d). Chlorite occurring in spinel core has a chromian-chlorite composition (e.g., Merlini et al., 2009) being characterized by Cr₂O₃ contents of ~ 3 wt% (Table 9). Chlorite rimming spinel porphyroblasts and in the groundmass have relatively low Cr₂O₃.

LATTICE PREFERRED ORIENTATION (TEXTURE) QUANTITATIVE ANALYSIS BY NEUTRON DIFFRACTION

We performed a study of the Lattice Preferred Orientation (LPO) of minerals with the main purpose of deciphering the deformation mechanisms that were active during the development of the pre-S₁ fabric in dunite samples. For such analysis, we selected sample ANT64 (dunite; see Table 1), one of the best preserved ultramafic rocks of the Antrona ophiolite. As already described in the structural paragraph and shown in Fig. 6, ANT 64 dunite sample mainly consists of olivine (Ol 90%), while opaque minerals, chlorite, ± serpentine constitute less than 10% of the rock. The pre-S₁ foliation is defined by the shape-preferred orientation of Ol. Olivine occurs as elongated and strained porphyroblasts (Ol_p).

The sliding dominant mechanism may be related to the physical conditions occurring during rock deformation; thus, the LPO analysis is essential for investigating the origin of rock foliation, namely whether it has developed during the Alpine tectonic evolution or during the mantle upwelling in the oceanic realm.

Table 6 - Representative microchemical composition of spinel.

Sample	ANT104	ANT104	ANT120	ANT120	ANT64	ANT64
Rock type	foliated S.	foliated S.	foliated S.	foliated S.	dunite	dunite
Analysis #	104-3-5	104-5-16	B-42	B-43	D-24	D-25
Texture	CpxI exol.	neoblasts aggr.	porphyroclast	porphyroclast	porphyroclast	porphyroclast
wt%						
SiO ₂	0.06	bdl	0.46	bdl	0.10	1.08
TiO ₂	0.62	1.25	0.42	0.75	0.92	0.78
Al ₂ O ₃	bdl	0.07	0.80	0.77	1.17	1.39
Cr ₂ O ₃	4.33	5.08	57.89	53.89	55.83	55.31
Fetot	87.99	87.73	35.39	39.76	36.94	34.78
MnO	0.10	0.21	0.56	0.54	0.68	0.66
MgO	0.49	0.83	1.94	1.74	2.60	3.23
CaO	0.23	bdl	bdl	bdl	bdl	0.02
ZnO	bdl	bdl	1.29	1.12	0.48	0.85
NiO	bdl	bdl	bdl	bdl	0.17	0.06
Ox Total	93.84	95.19	98.78	98.62	98.92	98.15
Normalization on the basis of 3 CATIONS and 8 CHARGES						
Fe ²⁺	1.000	1.000	1.000	1.000	1.000	1.000
Mn	0.004	0.009	0.018	0.018	0.022	0.021
Mg	0.036	0.060	0.110	0.100	0.147	0.181
Ca	0.012	-	-	-	-	0.001
Zn	-	-	0.036	0.032	0.013	0.024
Ni	-	-	-	-	0.005	0.002
A	1.053	1.068	1.165	1.151	1.188	1.228
Si	0.003	-	0.017	-	0.004	0.041
Ti	0.023	0.045	0.012	0.022	0.026	0.022
Al	-	0.004	0.036	0.035	0.052	0.061
Cr	0.169	0.194	1.734	1.645	1.670	1.642
Fe ³⁺	1.760	1.695	0.081	0.189	0.112	0.061
B	1.956	1.939	1.880	1.892	1.865	1.827
Cat Total	3.009	3.007	3.045	3.043	3.053	3.055
Cr/(Cr+Al)	-	97.99	97.99	97.92	96.98	96.39
Mg/(Mg+Fe ²⁺)	3.49	5.64	9.88	9.11	12.79	15.31

Cpx exol.- magnetite replacing exolutions inside clinopyroxene porphyroclasts.

Method

The nature and shape of LPO is controlled by both microscopic processes and macroscopic field geometry, as described by Karato (2008). The development of LPO in naturally deformed rocks is the sum of the microscopic deformation, that is linked to the internal distortion of crystals, and deformation of the mesoscopic crystal aggregates, coupled with the geometry of the strain field. The study of LPO natural rocks is therefore of great interest if one wants to infer the conditions of deformation of crystalline aggregates. In order to quantify the LPO of minerals, a neutron diffraction technique was here used. This technique allows to investigate volumes of rock of 1 cm³-volume in a short time (about 1 hour), thanks to the penetration of neutron in matter and to the high flux, available at the nuclear reactor at the Institute Laue-Langevin (Grenoble, France).

Quantitative Texture Analysis (QTA) using diffraction relies on the measurement of pole figures used as input for the determination of the Orientation Distribution Function

(ODF) of crystallites, which corresponds to the complete representation of the LPO of crystals in the tridimensional space. The minimum number of pole figures to be measured in order to be able to determine the ODF depends on the crystal symmetry and on the available experimental coverage for a given instrument (Wenk, 1985). Each of these pole figures requires the measurement of a large number of points, which depends on the scanning strategy and the wanted ODF resolution (Morawiec, 2004). For a typical scan and an ODF resolution of 5°x5°x5°, around 1400 measurement points are needed for each complete pole figure. This can give rise to high acquisition time if low-flux radiation is used or weakly diffracting samples are studied. Several authors then proposed to simultaneously measure several pole figures with the help of linear (Bunge et al., 1982) or Curved (Heizmann and Laruelle, 1986) Position Sensitive Detectors (PSD and CPS respectively) as firstly developed for x-ray instruments. Such a gain in acquisition time was even more crucially targeted in order to measure textures within reasonable times at neutron steady state reactors

Table 7 - Representative microchemical composition of serpentine.

Sample	ANT104	ANT104	ANT104	ANT104	ANT104	ANT104
Rock type	foliated S.					
Analysis #	104-2-26	104-4-12	A-7	B-13	C-20	C-21
Texture	acicular	in vein	groundmass	groundmass	near Oln	near Oln
wt%						
SiO ₂	43.35	44.07	42.00	41.60	41.44	41.41
TiO ₂	bdl	bdl	bdl	0.04	bdl	0.04
Al ₂ O ₃	2.15	1.30	2.54	2.94	3.13	3.24
Cr ₂ O ₃	0.08	0.10	0.21	0.36	0.07	0.38
FeO	4.49	4.08	4.69	4.33	4.56	4.54
MnO	0.08	bdl	0.04	bdl	bdl	0.03
MgO	38.13	38.54	36.43	36.41	36.29	36.43
CaO	bdl	bdl	bdl	bdl	bdl	bdl
NiO	bdl	bdl	0.19	0.23	0.23	0.16
Ox Total	88.28	88.09	86.09	85.92	85.72	86.23
Nomalization on the basis of 7 oxygens						
Si	2.01	2.04	1.996	1.980	1.978	1.967
Ti	-	-	-	0.002	-	0.001
Al IV	0.00	0.00	0.004	0.020	0.022	0.033
Al VI	0.12	0.07	0.138	0.145	0.154	0.149
Al	0.12	0.07	0.142	0.165	0.176	0.181
Cr	0.00	0.00	0.008	0.014	0.003	0.014
Fe ₂	0.17	0.16	0.186	0.172	0.182	0.180
Mn	0.00	-	0.001	-	-	0.001
Mg	2.63	2.65	2.581	2.584	2.582	2.580
Ca	-	-	-	-	-	-
Ni	-	-	0.007	0.009	0.009	0.006
Cat Total	4.93	4.93	4.922	4.925	4.930	4.932
Mg/(Mg+Fe ₂)	93.9	94.3	93.3	93.7	93.4	93.5

Oln- olivine neoblast.

(Bunge et al., 1982), spallation (Wenk et al., 1991) and hybrid (Ullemeyer et al., 1998) sources. The typical acquisition time for texture experiments then decreased from few days to few hours per sample, thanks to multidetector developments and sources efficiencies. Such gains in measuring times are particularly important when full diagrams are needed for each sample orientation in order to operate not only texture analysis but also structure-texture determination, as was initially called "Rietveld-Texture" (Wenk et al., 1994; Matthies et al., 1997) and later on "Combined" (Chateigner, 2010) analyses, for which point detectors would simply impose prohibitive acquisition time.

In this work we present results from D19 diffractometer at ILL (Institute Laue-Langevin, Grenoble France). This study also illustrates the possibilities of reducing the acquisition time for QTA, in a typical range of 120° in 2θ, by using a Curved Area Position Sensitive detector (CAPS).

We measured our samples making use of the new CAPS detector of the D19 diffractometer (Fig. 8), covering an an-

gular range of 120°x30° with spatial resolution of 0.19° horizontally and 0.12° vertically. Each detecting column covers an equivalent c-range of 30° to 60°, for a total detecting solid angle of roughly 1.1 sr. For this measurement, a wavelength of 1.46 Å was used, and the data reduction strategy consisted of intensity corrections, localisation corrections and combined analysis. This instrument is located as close to the neutron source, and the flux at the sample position is between 10⁷ to 10⁸ ncm⁻²s⁻¹.

Results

The LPO analyses were performed on samples of dunites and foliated serpentinites characterized by well preserved pre-S₁ structures; the investigation was aimed to support the interpretation regarding the pre-S₁ fabrics origin, likely related to the pre-Alpine mantle history.

Since the dunite samples (e.g., ANT64) are composed of olivine (> 95%), opaque minerals, chlorite, ± serpentine (see

Table 8 - Representative microchemical composition of amphibole.

Sample	ANT 104	ANT 104	ANT 120	ANT 120	ANT 120	ANT 120
Rock type	foliated S.	foliated S.	ol-cpx-am-rock	ol-cpx-am-rock	ol-cpx-amp-rock	ol-cpx-amp-rock
Analysis #	104-3-4	104-5-14	120-2-1	120-3-18	120-3-17	120-4-15
Texture	replacing Cpx p	neoblast	replacing Ol	pseudomorph (c)	pseudomorph (r)	neoblast
wt%						
SiO ₂	59.86	59.32	59.06	60.05	56.50	59.21
TiO ₂	bdl	bdl	0.05	0.04	0.08	bdl
Al ₂ O ₃	0.23	0.23	0.20	0.06	2.45	0.21
Cr ₂ O ₃	0.04	0.03	0.05	bdl	1.34	bdl
FeO	1.70	1.59	1.83	1.71	1.90	1.83
MnO	0.05	0.05	0.06	0.07	0.07	0.05
MgO	23.69	23.51	23.56	23.87	22.61	23.56
CaO	13.68	13.64	13.06	13.15	12.58	13.21
Na ₂ O	0.15	0.16	0.20	0.13	1.07	0.19
K ₂ O	bdl	bdl	bdl	bdl	0.02	0.02
Ox Total	99.40	98.53	98.07	99.08	98.62	98.28

Normalization on the basis of 23 oxygens

Si-T	8.04	8.04	8.05	8.09	7.66	8.05
Al (IV)	0.00	0.00	0.00	0.00	0.34	0.00
Tot-T	8.04	8.04	8.05	8.09	8.00	8.05
Al (VI)	0.04	0.04	0.03	0.01	0.05	0.03
Ti	-	-	0.01	0.00	0.01	-
Cr	0.00	0.00	0.01	-	0.14	-
Fe ₃₊	0.19	0.18	0.21	0.19	0.18	0.21
Mg	4.75	4.75	4.75	4.79	4.57	4.76
Fe ₂₊	0.00	0.00	0.00	0.00	0.03	0.00
Mn ₂₊	0.01	0.01	0.00	0.00	0.01	0.00
Tot-C	4.99	4.98	5.01	4.99	4.99	5.00
Mg	0.00	0.00	0.04	0.00	0.00	0.02
Mn ₂₊	0.00	0.00	0.01	0.01	0.00	0.01
Ca	1.97	1.98	1.91	1.90	1.83	1.92
Na	0.03	0.02	0.05	0.03	0.17	0.05
Tot-B	2.00	2.00	2.00	1.94	2.00	2.00
Na-A	0.01	0.02	0.00	0.00	0.11	0.00
K-A	-	-	-	-	0.00	0.00
Tot-A	0.01	0.02	0.00	0.00	0.11	0.00
Name	Tremolite	Tremolite	Tremolite	Tremolite	Tremolite	Tremolite

Cpx p- clinopyroxene porphyroclast; pseudom.- chl + am-pseudomorph replacing probable pyroxene in sample ANT120; c, r- core, rim.

Table 1) and are characterized by the SPO of Ol_p, which describes the pre-S₁ foliation, they are best suited for quantitative texture analysis by neutron diffraction (Zucali et al., 2002). The microscopic foliation (XY plane), is here taken as the main reference to the LPO geometry, as shown in Fig. 8. Olivine has an orthorhombic structure, space group Pbnm (N. 62) and the cell parameters used for the profile fitting and EWIMV refinement are a = 4.77 Å, b = 10.20 Å, c = 6.00 Å. Table 10 summarizes the analytical conditions to-

gether with reliability factors for Rietveld refinement and EWIMV calculation (Chateigner, 2005), where RW and RB correspond respectively to weighted and Bragg factors for Rietveld and ODF analysis. In particular, F2 (Table 10) corresponds to the Texture Index described for Quantitative Texture Analysis by Bunge (1982). The refinement quality was assessed by comparison of the experimental and recalculated diagrams (Fig. 9), and by the reliability factors (Table 10) as exhaustively described by Chateigner (2005).

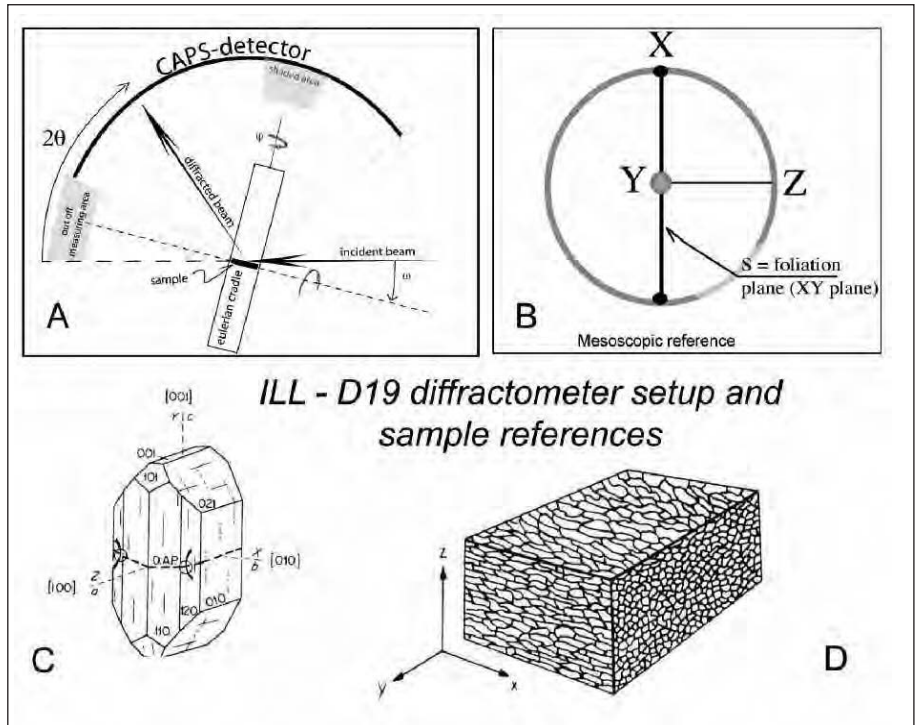


Fig. 8 - A) ILL D19 diffractometer; B) Mesoscopic fabric reference with respect to pole figure orientations; C) Crystallographic habit and optical directions of forsterite; D) Penetrative foliation and mineral lineation and how they relate to the mesoscopic fabrics.

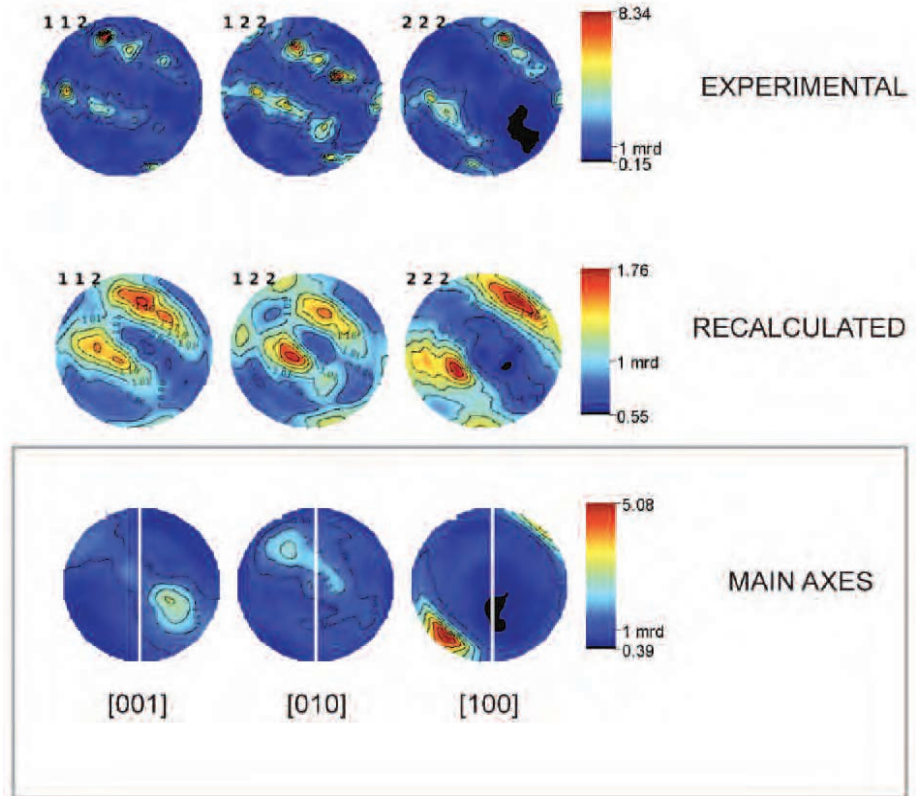


Fig. 9 - Graphical comparison of selected experimental and recalculated pole figures; orientation of the main lattice axes of olivine of ANT64 sample, represented on direct pole figures plots.

Fig. 9 shows pole figures for selected lattice planes of olivine in equal-area projection for dunite sample (ANT64); not all the pole figures used in the computation of the ODF are shown. Fig. 9a shows the experimental pole figures extracted using the Le Bail algorithm and the coverage of the orientation space. Fig. 9b shows the same pole figures recalculated from the ODF obtained by the EWIMV algorithm of MAUD and the orientation of the main direc-

tions of olivine, also calculated from the ODF.

The comparison between experimental and recalculated pole figures shows the goodness of the EWIMV solution for the ODF for both samples. The orientation of the main crystallographic axes (Fig. 9c) is characterized by strong maximum of the [100] axis, lying within the XZ plane and at about 40-45° to the foliation plane. This is confirmed by microscopic observations (see Fig. 5d). The [010] and [001]

Table 9 - Representative microchemical composition of chlorite.

Sample	ANT120	ANT120	ANT120	ANT120	ANT120	ANT64	ANT64
Rock type	ol-cpx-am-rock	ol-cpx-am-rock	ol-cpx-am-rock	ol-cpx-am-rock	ol-cpx-am-rock	dunite	dunite
Analysis #	C-3	B-44	B-45	A-49	A-50	D-27	D-28
Texture	ol rim	spl core	spl rim	groundmass	spl rim	spl rim	spl rim
wt%							
ZnO	0.10	bdl	bdl	0.09	bdl	bdl	0.13
MgO	33.38	33.55	32.91	34.08	33.57	34.04	33.63
Al ₂ O ₃	12.01	13.44	12.92	13.16	10.41	14.48	14.90
SiO ₂	34.11	33.41	34.38	34.79	34.90	34.33	33.87
K ₂ O	0.01	0.02	bdl	bdl	bdl	bdl	bdl
CaO	bdl	0.02	bdl	bdl	0.02	0.03	0.03
TiO ₂	bdl	bdl	0.07	0.05	bdl	0.09	0.06
Cr ₂ O ₃	0.88	3.25	1.35	0.37	2.69	0.43	0.04
MnO	bdl	bdl	bdl	bdl	bdl	bdl	0.06
FeO	3.22	3.41	3.46	3.05	3.44	2.66	2.81
NiO	0.22	0.22	0.15	0.23	0.29	0.22	0.20
Cl	bdl	bdl	bdl	bdl	bdl	bdl	bdl
Ox Total	83.93	87.32	85.25	85.82	85.32	86.28	85.73
Normalization on the basis of 28 oxygens							
Si	6.669	6.341	6.619	6.627	6.756	6.489	6.448
Al	2.767	3.006	2.931	2.954	2.375	3.225	3.343
Al iv	1.331	1.659	1.381	1.373	1.244	1.511	1.552
Al vi	1.436	1.347	1.551	1.581	1.130	1.714	1.791
Ti	-	-	0.011	0.007	-	0.013	0.008
Cr	0.136	0.488	0.206	0.056	0.412	0.064	0.006
Mn	-	-	-	-	-	-	0.010
Zn	0.015	-	-	0.013	-	-	0.018
Mg	9.730	9.493	9.446	9.678	9.688	9.592	9.545
K	0.003	0.005	-	-	-	-	-
Ca	-	0.004	-	-	0.004	0.006	0.007
Fe ₂	0.526	0.541	0.557	0.486	0.557	0.420	0.447
Ni	0.034	0.033	0.024	0.036	0.046	0.033	0.030
Tot Cat	15.945	16.543	16.083	16.147	15.410	16.545	16.728

Minerals abbreviations according to Siivola and Schmid (2007).

Table 10 - ODF refinement estimators: RW, Intensity weighted factor.

Sample description		Instrument		Rietveld			EWIMV	
		Line	wavelength (Å)				F2	min_int (% of max.)
		D19 - ILL Grenoble						
sample	mineralogy	RW	RB	RW	RB	Rexp	F2	min_int (% of max.)
ant64b	Ol 100%	61.84	51.16	18.69	13.67	17.14	1.79	0.1

RB, R-Bragg factor. Rietveld-profile refinement estimators: RW, R-weighted pattern factor; RB, R-pattern factor; Rexp. EWIMV: F2, Texture Index, resolution, ODF resolution in degrees; min_int, minimum intensity used for ODF calculations, as % of maximum measured intensity.

axes distribution defines a girdle perpendicular to the XZ plane containing the Y direction and at about 45° to the foliation plane. Moreover the girdle distribution is characterized by two maxima at about 90° each other and describing an angle of 45° with the Y axis. Similar orientation for the main axes of olivine were described by several authors as characteristic of type D and E distribution (Drury, 2005; Karato et al., 2008 and reference therein).

The relationships between the olivine fabric and the dominant slip systems suggest [100](0kl) and [100](001) as active slip systems (Karato et al., 2008). The activation of this slip system is referred as possible at $T > 800^{\circ}\text{C}$ for $P = 1.5$ (Carter and Ave'lallemant, 1970) and it is sensitive to the pressure increase, since variation in active slip system is referred for forsterite single crystal at $P > 5\text{GPa}$ (Raterron et al., 2009). Water content and stress also influence the activation of slip system, where E-type corresponds to water content of 200 to 1000 p.p.m. H/Si (50-250 p.p.m. wt.) and stress range of 0-400 Mpa, and D-type LPO are described at high stress conditions (400-500MPa) and very low water contents (< 200 p.p.m. H/Si and 100 p.p.m. wt) (Karato et al., 2008). LPO geometry with respect to shear plane and foliation plane directions may be related to strain states as proposed by Tommasi et al. (2000) and Warren et al. (2008). In our samples the only reference is the foliation plane and the lineation direction, while no informations about to shear plane orientation are available. This restriction complicates a reliable evaluation of the strain state during LPO development; however, the angle between [100] maxima and the plane of the mesoscopic foliation and the preferred cluster distribution of the main axes (Fig. 9) suggest a constrictional simple shear geometry of the mesoscopic strain field under a relatively low shear strain, which does not exceed 100-140% of shear strain (Warren et al., 2008).

DISCUSSION

The ultramafic rocks of the Antrona ophiolite exposed in the lower Loranco Valley mainly consist of serpentinitized peridotites with minor interbedded mafic/ultramafic rocks occurring as layers, boudins or pods, namely, cm-scale cpx-rich layers, amphibole-bearing chloriteschists, dunites, amphibole-rich layers, and chloriteschists. On the basis of field observations, these rocks underlie amphibolites and metasediments, thus constituting a sole for the volcanic and cover sequence of the Antrona ophiolite. In the marginal parts of the ultramafic massif, the ultramafites are in contact with flaser metagabbros grading to mylonitic amphibolites near the main tectonic contact with the Camughera-Moncucco Unit, consisting of orthogneiss. Given the pervasive transposition produced during the Alpine tectonics, the contacts between different lithologies are considered tectonic.

Origin of the Antrona serpentinites as inferred from microstructures and quantitative texture analysis

In spite of the tectonic and metamorphic evolution of the Antrona ophiolite, mostly related to the Alpine history (Colombi and Pfeifer, 1986; Colombi, 1989; Pfeifer et al., 1989; Turco and Tartarotti, 2006), and in spite of the heavy serpentinitization, the ultramafic rocks preserve relict microstructures, textures and mineralogy that allow discussing the nature of their protoliths.

While mylonitic serpentinites have a reworked texture and

consist of only serpentine (+ magnetite), foliated serpentinites mineral assemblage includes olivine, pyroxene, and spinel (\pm magnetite). Among unaltered minerals, olivine and clinopyroxene porphyroblasts (Ol_p and Cpx_p) represent the best preserved mineral phases, occurring in less recrystallized samples. Ol_p and Cpx_p are here interpreted as possible mantle relics, as suggested by their microstructural and textural features. In fact, the occurrence of subgrains inside Ol_p , recalling intracrystalline “kink-bands” (Mercier and Nicolas, 1975) or “deformation lamellae” (Den Tex, 1969; Mercier and Nicolas, 1975) may be referred to intracrystalline deformation, i.e., to dislocation alignment forming along parallel glide lines within the crystal, commonly found in mantle peridotites. Exsolved Cpx_p is also typically found in mantle peridotites (e.g., Gueguen and Nicolas, 1980; Tartarotti et al., 2002; Dick et al., 2010), although in our samples the exsolution lamellae are always replaced by opaque minerals. Other relict minerals or textures are: *i*) porphyroclastic holly-leaf-shaped spinel, which is typically found in porphyroclastic mantle peridotites; *ii*) mm-scale pseudomorphs consisting of serpentine in serpentinites, and of chl + am in coarse-grained ol-cpx-spl (\pm am, \pm chl)-rich rocks, that we interpret as secondary minerals replacing earlier (ortho?)pyroxene porphyroclasts. The Antrona foliated serpentinites may thus preserve relict (pre-Alpine) mantle porphyroclastic textures, although crystal-plastic recrystallization with neoblasts formation related to the Alpine orogenic history cannot be completely ruled out. In order to unravel the main question of a possible mantle origin of serpentinite samples, a LPO study by Quantitative Texture Analysis (QTA) using neutron diffraction was carried out in rock samples containing strained olivine crystals. The relationship between the analyzed olivine fabric and the dominant slip systems suggests [100](0kl) and [100](001) as active slip systems (Karato et al., 2008). The activation of these slip systems is referred as possible at $T > 800^{\circ}\text{C}$ for $P = 1.5$ GPa (Carter and Ave'lallemant, 1970) although it is sensitive to a pressure increase (e.g., Raterron et al., 2009). This result suggests that the olivine fabric in the studied samples has been inherited from the pristine mantle structure, since temperature values as high as 800°C have never been estimated for the Antrona ophiolite. The Antrona serpentinitized ultramafic rocks are thus interpreted as relict portions of mantle tectonites. Similar interpretations, although not supported by quantitative fabric analyses, have been advanced for other few serpentinite bodies in the Alpine metaophiolites, namely, the Mount Avic serpentinites (Tartarotti and Martin, 1991; Diella et al., 1994; Fontana et al., 2008), the Zermatt-Saas serpentinites (Li et al., 2004), and the southern Lanzo ophiolitic massif (e.g., Piccardo et al., 2005).

On the basis of petrographic and textural characters, we interpret the clinopyroxene-rich layers and amphibole-bearing chloriteschists associated with serpentinites as deriving either from original mantle pyroxenites, then transformed to chlorite-rich rocks during the Alpine orogenic evolution, or from original (Mg-rich?)-gabbros, interbedded within serpentinites by tectonic transposition, as suggested by the occurrence of metagabbro outcrops very close to the serpentinite massif (see Fig. 2). In this view, the chloriteschists may derive by a complete obliteration of texture and mineralogy (by metasomatic reactions?) of previous gabbros. Similar clinopyroxene (mainly diopside) + chlorite-rich layers have been described in the Mount Avic serpentinite massif (Western Alps ophiolites; Panseri et al., 2008) and interpreted as deriving from original intrusives. The dunite layers in the Antrona serpentinites likely represent original residual

dunites hosted in the mantle harzburgite/lherzolite main body. The amphibole-rich layers are the only rocks that include plagioclase. We infer that these layers represent original mafic intrusions within hosting mantle peridotites, although there are no evidence of rodingitic minerals.

Inferences from mineral composition

Field observations integrated by thin-section investigations of the Antrona ultramafic rocks suggest that serpentinized peridotites are the dominant rock type. They include: *i*) foliated serpentinites characterized by (more or less) transposed S_1 foliation consisting of olivine (Ol_p , Ol_n), clinopyroxene (Cpx_p , Cpx_n), spinel, serpentine (e.g., sample ANT104); *ii*) less intensely deformed serpentinites, consisting of coarse-grained ol-cpx-spl (\pm am, \pm chl replacing orthopyroxene?) -rich rocks (e.g., sample ANT120); *iii*) mylonitic serpentinites. Textural and petrographic features suggest that these rocks consist of partly serpentinized harzburgites or lherzolites. Microchemical analyses reveal that olivine has a variable composition, since forsterite in Ol_p and Ol_n ranges between Fo_{87} and Fo_{88} (Fo_{90} was found only in dunites). Such composition is partly comparable with that of abyssal peridotites from modern oceanic lithosphere which commonly have $Fo\%$ ranging between Fo_{89} and Fo_{90} (e.g., Dick, 1989; Tartarotti et al., 2002; Seyler et al., 2003; Dick et al. 2010; Warren and Shimizu, 2010). Clinopyroxene porphyroblasts are relatively richer in Al_2O_3 and Cr_2O_3 with respect to clinopyroxene neoblasts and retain a composition comparable with that of clinopyroxene from modern plagioclase-free abyssal peridotites (e.g., Dick, 1989; Warren and Shimizu, 2010). We infer that iron-enrichment in olivine (and slight calcium-enrichment in clinopyroxene) could be related to rock recrystallization during the Alpine orogenic evolution. Spinel composition in our samples ranges between pure magnetite to ferritchromite. While magnetite (e.g., sample ANT104) shows a completely reworked texture if compared with that of typical mantle spinel, the spinel crystals with a (Ti-poor)-ferritchromite composition show a holly-leaf habit, which is a typical shape for spinel in porphyroclastic mantle peridotites (Mercier and Nicolas, 1975). However, ferritchromite composition is not comparable with that commonly found in abyssal peridotite spinel (e.g., Dick, 1989; Hébert et al., 1989). By contrast, similar ferritchromite-rich spinel characterized by a porous texture and a Cr-chlorite rim (like that found in our samples; see Table 7) has been described in some localities, such as the Kalkan Ophiolite of the southern Urals, and interpreted as being due to alteration and metamorphic overprints on former chromite (Merlini et al., 2009). The most likely environment suggested by these Authors for such alteration is a prograde metamorphic event post-dating serpentinization, possibly related to emplacement within an accretionary wedge. The relatively low Ti content of the analyzed ferritchromite in the coarse-grained peridotites (sample ANT120) and in dunites (sample ANT64) allows us to rule out a cumulate nature of the host rock (e.g., Hébert et al., 1989). Consequently, the shape and composition of the analyzed spinel, namely the relict holly-leaf habit and the Cr-rich, Ti-poor chemistry, support the hypothesis of a mantle origin for the Antrona serpentinites.

The quantitative texture analysis carried out on dunite samples strongly supports this hypothesis, by constraining the temperature interval that accompanied the activation of olivine slip system.

SUMMARY AND CONCLUSIONS

Summing up, we suggest that the Antrona ultramafic body derives from original mantle harzburgites and/or lherzolites associated with dunite pods and possibly pyroxenite layers. The chemical composition of the analyzed olivine and clinopyroxene porphyroblasts suggests a sub-oceanic nature for these mantle-derived rocks which thus represent the mantle portion of the Antrona ophiolite. This fossilized fragment of oceanic lithosphere has been involved in several geodynamic steps, from its emplacement in the Jurassic Tethys to subduction and suture in the Alpine chain. Tectonic transposition has obliterated the primary structures of the Tethyan lithosphere, thus preventing a clear interpretation of the original stratigraphy. However, we envisage that the mantle portion of the Antrona ophiolite may have been intruded by original mafic dykes and plutons (of unknown size), now coupled by tectonic contacts. This scenario is comparable to that envisaged for the Mount Avic serpentinite massif (Tartarotti and Martin, 1991; Fontana et al., 2008; Panseri et al., 2008), excepting the scarce occurrence of rodingites in the Antrona area.

Although its extension is smaller, the Antrona ophiolite seems to be comparable with a coherent ophiolitic slice, such as Zermatt Saas ophiolite (e.g., Angiboust et al., 2011 and references therein), more than with a serpentinite mélange. However, further investigations, namely detailed P-T paths, are needed to better constrain the internal setting of the Antrona ophiolite and compare them with other well studied ophiolites of the Alpine chain.

ACKNOWLEDGEMENTS

This project was funded by PRIN 2008 grants. We are grateful to Laura Crispini and Stephane Guillot for their helpful comments and review of the manuscript.

REFERENCES

- Amato J.M., Johnson C.M., Baumgartner L.P. and Beard B.L., 1999. Rapid exhumation of the Zermatt-Saas ophiolite deduced from high-precision Sm-Nd and Rb-Sr geochronology. *Earth Planet. Sci. Lett.*, 171: 425-438.
- Angiboust S., Agard P., Jolivet L. and Beyssac O., 2009. The Zermatt-Saas ophiolite: the largest (60-km wide) and deepest (c. 70-80 km) continuous slice of oceanic lithosphere detached from a subduction zone? *Terra Nova*, 21: 171-180.
- Angiboust S., Langdon R., Agard P., Waters D. and Chopin C., 2011. Eclogitization of the Monviso ophiolite (W. Alps) and implications on subduction dynamics. *J. Metam. Geol.*, doi:10.1111/j.1525-1314.2011.00951.x
- Argand E., 1911. Le nappes de recouvrement des Alpes occidentales et les territoires environnants. *Essai de carte structurale* 1:500.000. *Carte spéc.*, n. 64.
- Bailey S.W., 1988a. Chlorites: Structures and crystal chemistry. *Rev. Mineral. Geochem.*, 19: 347-403.
- Bailey S.W., 1988b. Structures and compositions of other trioctahedral 1:1 phyllosilicates. *Rev. Mineral. Geochem.*, 19: 169-188.
- Bailey S.W., Banfield J.F., Barker W.W. and Katchan G., 1995. Dozyite, a 1:1 regular interstratification of serpentine and chlorite. *Am. Mineral.*, 80: 65-77.
- Barnicoat A.C. and Fry N., 1986. High-pressure metamorphism of the Zermatt-Saas ophiolite zone, Switzerland. *J. Geol. Soc.*, 143: 607-618.
- Bearth P., 1952. *Geologie und Petrographie des Monte Rosa*. *Beitr. Geol. Karte Schweiz* 96, 94 pp.

- Bearth P., 1954. Geologischer Atlas der Schweiz 1:25.000, Blatt Saas (Nr. 30) und Blatt Monte Moro (Nr. 31). Schweiz. Geol. Kommission.
- Bearth P., 1956. Zur geologie der Wurzelzone östlich des Ossolates. *Ecl. Geol. Helv.*, 49: 267-278.
- Bearth P., 1957. Erläuterungen zum Blatt Saas und Monte Moro. Schweiz. Geol. Kommission.
- Bigoggero B., Boriani A., Colombo A. and Tunesi A., 1981. Età e caratteri petrochimici degli ortogneiss della zona Moncucco-Orselina nell'area Ossolana. *Rend. Soc. It. Mineral. Petrogr.*, 38: 207-218.
- Blake M.C., Moore D.E. and Jayko A.S., 1995. The role of serpentinite mélanges in the unroofing of ultrahigh-pressure metamorphic rocks: An example from the Western Alps in Italy. In: R.G. Coleman and X. Wang (Eds.), *Ultrahigh pressure metamorphism*. Cambridge Univ. Press, Cambridge, p. 182-205.
- Blumenthal M.M., 1952. Beobachtungen über den Bau und Verlauf der Muldenzone von Antrona. *Ecl. Geol. Helv.*, 45: 20-251.
- Bonatti E. and Michael, P.J., 1989. Mantle peridotites from continental rifts to ocean basins to subduction zones. *Earth Planet. Sci. Lett.*, 91: 297-311.
- Borghi A., Compagnoni R. and Sandrone R., 1996. Composite P-T paths in the Internal Penninic Massifs of the Western Alps: Petrological constraints to their thermo-mechanical evolution. *Ecl. Geol. Helv.*, 89: 345-367.
- Bowtell S.A., Cliff R.A. and Barnicoat C., 1994. Sm-Nd isotopic evidence on the age of eclogitization in the Zermatt-Saas ophiolite. *J. Metam. Geol.*, 12: 187-196.
- Bucher K., Fazis Y., de Capitani C., and Grapes R., 2005. Blueschists, eclogites, and decompression assemblages of the Zermatt-Saas ophiolite: High-pressure metamorphism of subducted Tethys lithosphere. *Am. Mineral.*, 90: 821-835.
- Bunge H.J. and Esling C., 1982. Quantitative Texture Analysis. *Deutsche Gesellsch. Metallkunde*, 551 pp.
- Bunge H.J., Wenk H.R. and Pannetier J., 1982. Neutron diffraction texture analysis using a 2q position sensitive detector. *Textures Microstr.*, 5: 153-170.
- Carrupt E. and Schlup M., 1998. Métamorphisme et tectonique du versant sud du Val Bognanco (Pennique, Alpes italiennes). *Bull. Soc. Vaudoise Sci. Nat.*, 86: 29-59.
- Carter N.L. and Ave'lallemant H.G., 1970. High temperature flow of dunite and peridotite. *Geol. Soc. Am. Bull.*, 81: 2181-2202.
- Castelli D. and Lombardo B., 2007. The plagiogranite FeTi-Oxide gabbro association of Verné (Monviso metamorphic ophiolite, Western Alps). *Ophioliti*, 32: 1-14.
- Chateigner D., 2005. Reliability criteria in quantitative texture analysis with experimental and simulated orientation distributions. *J. Appl. Crystall.*, 38: 603-611.
- Chateigner D., 2010. Combined analysis. ISTE Ltd and John Wiley & Sons Inc, 496 pp.
- Chernosky J.V. Jr., Berman R.G. and Bryndzia L.T., 1988. Stability, phase relations, and thermodynamic properties of chlorite and serpentine group minerals. *Rev. Mineral. Geochem.*, 19: 295-346.
- Colombi A., 1989. Métamorphisme et géochimie des roches mafiques des Alpes ouest-centrales (géoprofil Viège-Domodossola-Locarno). *Mém. Géol.*, Lausanne, 4: 1-216.
- Colombi A. and Pfeifer H.-R., 1986. Ferrogabbroic and basaltic meta-eclogites from the Antrona mafic-ultramafic complex and the Centovalli-Locarno region (Italy and Southern Switzerland) - first results. *Schweiz. Mineral. Petrogr. Mitt.*, 66: 99-110.
- Compagnoni R., Dal Piaz G.V., Hunziker J.C., Gosso G., Lombardo B. and Williams P.F., 1977. The Sesia-Lanzo zone, a slice of continental crust with alpine high pressure-low temperature assemblages in the Western Italian Alps. *Rend. Soc. It. Mineral. Petrogr.*, 33: 281-334.
- Dal Piaz G.V., 1964. Il cristallino antico del versante meridionale del Monte Rosa, paraderivati a prevalente metamorfismo alpino. *Rend. Soc. Mineral. It.*, 20: 101-135.
- Dal Piaz G.V., 1966. Gneiss ghiandoni, marmi ed anfiboliti antiche del ricoprimento Monte Rosa nell'alta Valle d' Ayas. *Boll. Soc. Geol. It.*, 85: 103-132.
- Dal Piaz G.V., 1993. Evolution of Austro-Alpine and Upper Penninic basement in the northwestern Alps from Variscan convergence to post-Variscan extension. In: J. von Raumer and F. Neubauer (Eds.), *Pre-Mesozoic geology in the Alps*. Springer-Verlag, p. 327-344.
- Dal Piaz G.V., 2001. Geology of the Monte Rosa massif: historical review and personal comments. *Schweiz. Mineral. Petrogr. Mitt.*, 81: 275-303.
- Dal Piaz G.V. and Lombardo B., 1986. Early-Alpine eclogite metamorphism in the Penninic Monte Rosa-Gran Paradiso basement nappes of the north-western Alps. *Geol. Soc. Am. Mem.*, 164: 249-265.
- Dal Piaz G.V., Hunziker J.C. and Martinotti G., 1972. La Zona Sesia-Lanzo e l'evoluzione tettonico-metamorfica delle Alpi nordoccidentali interne. *Mem. Soc. Geol. It.*, 11: 433-466.
- Dal Piaz G.V., Cortiana G., Del Moro A., Martin S., Pennacchioni G. and Tartarotti P., 2001. Tertiary age and paleostructural inferences of the eclogitic imprint of the Austroalpine outliers and Zermatt-Saas ophiolite, Western Alps. *Intern. J. Earth Sci.*, 90: 668-684.
- Den Tex E., 1969. Origin of ultramafic rocks, their tectonic setting and history: a contribution to the discussion of the paper: "The origin of ultramafic and ultrabasic rocks" by P.J. Wyllie. *Tectonophysics*, 7: 457-488.
- Dick H.J.B., 1989. Abyssal peridotites, very slow spreading ridges and oceanic ridge magmatism. In: A.D. Sanders and M.J. Morris (Eds.), *Magmatism in the ocean basins*, *Geol. Soc. London Spec. Publ.*, 42: 71-105.
- Dick H.J.B., Lissenberg C.J. and Warren J.M., 2010. Mantle melting, melt transport, and delivery beneath a slow-spreading ridge: the Paleo-MAR from 23°15'N to 23°45'N. *J. Petrol.*, 51: 425-467.
- Diella V., Ferrario A. and Rossetti P., 1994. The magnetite ore deposits of the southern Aosta valley: chromitite transformed during an Alpine metamorphic event. *Ophioliti*, 19: 247-256.
- Droop J.T.R., 1987. A general equation for estimating Fe³⁺ concentrations in ferromagnesian silicates and oxides from microprobe analyses, using stoichiometric criteria = Equation générale pour l'estimation de la concentration du fer ferrique dans les silicates et des oxydes ferromagnésiens à partir de l'analyse par microsonde électronique en utilisant des critères stœchiométriques. *Mineral. Maga.*, 51: 431-435.
- Drury M.R., 2005. Dynamic recrystallization and strain softening of olivine aggregates in the laboratory and the lithosphere. *Geol. Soc. London Spec. Publ.*, 243: 143-158.
- Ernst W. G. and Dal Piaz G.V., 1978. Mineral parageneses of eclogitic rocks and related mafic schists of the Piemonte ophiolite nappe, Breuil-St.Jacques area, Italian Western Alps. *Am. Mineral.*, 63: 621-640.
- Escher A., Masson H. and Steck A., 1987. Coupes géologiques des Alpes occidentales suisses. *Service hydrol. géol. national, Berne, Rapports géol.* 2, 11 pp.
- Escher A., Masson H. and Steck A., 1993. Nappe geometry in the Western Swiss Alps. *J. Struct. Geol.* 15: 501-509.
- Escher A., Hunziker J.C., Marthaler M., Masson H., Sartori M. and Steck A., 1997. Geologic framework and structural evolution of the western Swiss-Italian Alps. In: O.A. Pfiffner, P. Lehner, P. Heitzmann, St. Müller and A. Steck (Eds.), *Deep structure of the Swiss Alps*, Birkhäuser Verlag, Basel, p. 205-221.
- Federico L., Crispini L., Scambelluri M. and Capponi G., 2007. Ophiolite mélange zone records exhumation in a fossil subduction channel. *Geology*, 35: 499-502.
- Fontana E., Panseri M. and Tartarotti P., 2008. Oceanic relict textures in the Mount Avic serpentinites, Western Alps. *Ophioliti*, 33: 105-118.
- Frey M., Hunziker J.C., Frank W., Bocquet J., Dal Piaz G.V., Jäger E. and Niggli E., 1974. Alpine metamorphism of the Alps: a review. *Schweiz. Mineral. Petrogr. Mitt.*, 54: 247-290.

- Frey M., Hunziker J.C., O'Neil J.R. and Schwander H.W., 1976. Equilibrium-disequilibrium relations in the Monte Rosa granite, western Alps: petrological, Rb-Sr and stable isotope data. *Contrib. Mineral. Petrol.*, 55: 147-179.
- Froitzheim N., 1997. Mesozoic paleogeography and Alpine tectonics along transects in eastern and western Switzerland - Consequences of the origin of the Monte Rosa nappe. 3rd Workshop on Alpine Geol. Studies. *Quad. Geodin. Alpina Quatern.*, 4: 53-54.
- Froitzheim N., 2001. Origin of the Monte Rosa nappe in the Pennine Alps - A new working hypothesis. *Geol. Soc. Am. Bull.*, 113: 604-614.
- Gosso G., Dal Piaz G.V., Piovano V. and Polino R., 1979. High pressure emplacement of early-alpine nappes, postnappe deformations and structural levels. *Mem. Ist. Geol. Mineral., Univ. Padova*, 32, 15 pp.
- Gueguen Y. and Nicolas A., 1980. Deformation of mantle rocks. *Ann. Rev. Earth Planet. Sci.*, 8: 119-144.
- Guillot S., Schwartz S., Hattori K., Auzende A. and Lardeaux J.M., 2004. The Monviso ophiolitic Massif (Western Alps), a section through a serpentinite subduction channel. Evolution of the western Alps: insights from metamorphism, structural geology, tectonics and geochronology. *The Virtual Explorer*, 16. Paper 6.
- Hébert R., Serri G. and Hékinian R., 1989. Mineral chemistry of ultramafic tectonites and ultramafic to gabbroic cumulates from the major oceanic basins and Northern Apennine ophiolites (Italy) - A comparison. *Chem. Geol.*, 77: 183-207.
- Heitzmann J.J. and Laruelle C., 1986. Simultaneous measurement of several X-ray pole figures. *J. Appl. Crystall.*, 19: 467-472.
- Hunziker J.C., 1970. Polymetamorphism in the Monte Rosa, Western Alps. *Ecl. Geol. Helv.*, 63: 151-161.
- Jaboyedoff M., Béglé P. and Lobrinus S., 1996. Stratigraphie et évolution structurale de la zone de Furgg, au front de la nappe du Mont-Rose. *Bull. Soc. Vaudoise Sci. Nat.*, 84: 191-210.
- Karato S., 2008. Deformation of Earth materials: an introduction to the rheology of solid Earth, Cambridge Univ. Press, 463 pp.
- Karato S., Jung H., Katayama I. and Skemer P., 2008. Geodynamic significance of seismic anisotropy of the upper mantle: new insights from laboratory studies. *Ann. Rev. Earth Planet. Sci.*, 36, 59 pp.
- Keller L.M. and Schmid S.M., 2001. On the kinematics of shearing near the top of the Monte Rosa nappe and the nature of the Furgg zone in Val Loranco (Antrona Valley, N. Italy). Tectonometamorphic and paleogeographical consequences. *Schweiz. Mineral. Petrogr. Mitt.*, 81: 347-367.
- Keller L.M., Hess M., Fügenschuh B. and Schmid S.M., 2005a. Structural and metamorphic evolution of the Camughera-Moncucco, Antrona and Monte Rosa units southwest of the Simplon line, Western Alps. *Ecl. Geol. Helv.*, 98: 21-52.
- Keller L.M., Abart R., Schmid S.M. and De Capitani C., 2005b. Phase relations and chemical composition of phengite and paragonite in pelitic schists during decompression: a case study from the Monte Rosa Nappe and Camughera-Moncucco Unit, Western Alps. *J. Petrol.*, 46: 2145-2166.
- Kramer J., 2002. Structural evolution of the Penninic Units in the Monte Rosa region (Swiss and Italian Alps). Ph.D. Dissert., Univ. Basel, Switzerland, 154 pp.
- Laduron D., 1976. L'antiforme de Vanzone. Etude pétrologique et structurale dans la Valle Anzasca (Province de Novara, Italie). *Mém. Inst. Géol., Univ. Louvain*, 121 pp.
- Laduron D. and Merlin M., 1974. Evolution structurale et métamorphique de l'antiforme de Vanzone (Valle Anzasca, Prov. de Novara, Italie). *Bull. Soc. Géol. France*, 16: 264-265.
- Lagabrielle Y. and Cannat M., 1990. Alpine Jurassic ophiolites resemble the modern central Atlantic basement. *Geology*, 18: 319-322.
- Lagabrielle Y. and Lemoine M., 1997. Alpine, Corsican and Apennine ophiolites: the slow-spreading ridge model. *C. R. Acad. Sci., Series IIA, Earth Planet. Science*, 325: 909-920.
- Leake B.E., Woolley A.R., Arps C.E.S., Birch W.D., Gilbert M.C., Grice J.D. et al., 1997. Nomenclature of amphiboles: report of the Subcommittee on Amphiboles of the International Mineralogical Association, Commission on New Minerals and Mineral Names. *Am. Mineral.*, 82: 1019-1037.
- Li X.P., Rahn M. and Bucher K., 2004. Serpentinities of the Zermatt-Saas ophiolite complex and their texture evolution. *J. Metam. Geol.*, 22: 159-177.
- Lombardo B., Nervo R., Compagnoni R. et al., 1978. Osservazioni preliminari sulle ofioliti metamorfiche del Monviso (Alpi occidentali). *Rend. Soc. It. Mineral. Petrol.*, 34: 253-305.
- Martin S. and Tartarotti P., 1989. Polyphase HP metamorphism in the ophiolitic glaucophanites of the lower St. Marcel Valley (Aosta valley). *Ophioliti*, 14: 135-156.
- Matthies S., Lutterotti L. and Wenk H.R., 1997. Advances in texture analysis from diffraction spectra. *J. Appl. Crystall.*, 30: 31-42.
- Mercier J.-C.C. and Nicolas A., 1975. Textures and fabrics of upper-mantle peridotites as illustrated by xenoliths from basalts. *J. Petrol.*, 16: 454-487.
- Merlini A., Grieco G. and Diella V., 2009. Ferritchromite and chromian-chlorite formation in mélange-hosted Kalkan chromitite (Southern Urals, Russia). *Am. Mineral.*, 94: 1459-1467.
- Michard A., Goffé B., Chopin Ch. and Henry C., 1996. Did the Western Alps develop through an Oman-type stage? The geotectonic setting of high-pressure metamorphism in two contrasting Tethyan transects. *Ecl. Geol. Helv.*, 89: 43-80.
- Milnes A.G., Grellier M. and Müller R., 1981. Sequences and style of major post-nappe structures, Simplon-Pennine Alps. *J. Struct. Geol.*, 3: 411-420.
- Morawiec A., 2004. Orientations and rotations: computations in crystallographic textures. Springer Verlag, 210 pp.
- Nelson B.W. and Roy R., 1958. Synthesis of the chlorites and their structural and chemical constitution. *Am. Mineral.*, 43: 707-725.
- Nicolas A. and Poirier J.P., 1976. Crystalline plasticity and solid state flow in metamorphic rocks. John Wiley & Sons, London, 444 pp.
- Oberhansli R., 1980. P-T Bestimmungen anhand von Mineralanalysen in Eklogiten und Glaukophaniten der Ophiolite von Zermatt. *Schweiz. Mineral. Petrogr. Mitt.*, 60: 215-235.
- Panseri M., Fontana E. and Tartarotti P., 2008. Evolution of rodingitic dykes: metasomatism and metamorphism in the Mount Avic serpentinites (Alpine Ophiolites, southern Aosta Valley). *Ophioliti*, 33: 165-185.
- Pfeifer H.R., Colombi A. and Ganguin J., 1989. Zermatt-Saas and Antrona zone: A petrographic and geochemical comparison of polyphase metamorphic ophiolites of the western-central Alps. *Schweiz. Mineral. Petrogr. Mitt.*, 69: 217-236.
- Piccardo G.B., Zanetti A., Spagnolo G. and Poggi E., 2005. Recent researches on melt-rock interaction in the Lanzo South peridotite. *Ophioliti*, 30: 135-160.
- Raterson P., Amiguet E., Chen J., Li L. and Cordier P., 2009. Experimental deformation of olivine single crystals at mantle pressures and temperatures. *Phys. Earth Planet. Inter.*, 172: 74-83.
- Reinecke T., 1991. Very-high-pressure metamorphism and uplift of coesite-bearing metasediments from the Zermatt-Saas zone, Western Alps. *Eur. J. Mineral.*, 3: 7-17.
- Reinecke T., 1998. Prograde high to ultrahigh pressure metamorphism and exhumation of oceanic sediments at Lago di Cignana, Zermatt Saas Zone, Western Alps. *Lithos*, 42: 147-190.
- Seyler M., Cannat M. and Mével C., 2003. Evidence for major-element heterogeneity in the mantle source of abyssal peridotites from the Southwest Indian Ridge (52° to 68°E). *Geochem. Geophys. Geosyst.*, 4 (2), doi:10.1029/2002GC000305.
- Siivola J. and Schmid R., 2007. List of mineral abbreviations - Recommendations by the IUGS Subcommittee on the Systematics of Metamorphic Rocks. Electronic Source: <http://www.bgs.ac.uk/scmr/home.html>
- Steck A., Epard J.-L., Escher A., Lehner P., Marchant R. and Masson H., 1997. Geological interpretation of the seismic profile through Western Switzerland: Rawil (W1), Val d'Anniviers (W2), Matternal (W3), Zmutt-Zermatt-Findelen (W4) and Val de Bagnes (W5). In: O.A. Pfiffner, P. Lehner, P. Heitzmann, St. Müller and A. Steck (Eds.), *Deep structure of the Swiss Alps*. Birkhäuser Verlag, Basel, pp. 123-137.

- Steck A., Epard J.-L., Escher A., Gouffon Y. and Masson H., 2001. Carte tectonique des Alpes de Suisse occidentale et des régions avoisinantes 1:100,000. Notice explicative, Office fédérale eaux géologie, 73 pp.
- Tartarotti P. and Martin S., 1991. Ultramafic rocks in the Mount Avic eclogitic ophiolites, Italian Western Alps. *Terra Abstr.*, 3: 96.
- Tartarotti P., Benciolini L., Monopoli B., 1998. Breccie serpentinitiche nel massiccio ultrabásico del Monte Avic (Falda Ofiolitica Piemontese): possibili evidenze di erosione sottomarina. *Atti Ticiensi. Sci.Terra (Serie speciale)*, 7: 73-86.
- Tartarotti P., Susini S., Nimis P. and Ottolini L., 2002. Melt migration in the upper mantle along the Romanche Fracture Zone (Equatorial Atlantic). *Lithos*, 63: 125-149.
- Tommasi A., Mainprice D., Canova G. and Chastel Y., 2000. Viscoplastic self-consistent and equilibrium-based modeling of olivine lattice preferred orientations: Implications for the upper mantle seismic anisotropy. *J. Geophys. Res. Solid Earth*, 105: 7893-7908.
- Turco F. and Tartarotti P., 2006. The Antrona nappe: lithostratigraphy and metamorphic evolution of ophiolites in the Antrona Valley (Pennine Alps). *Ofioliti, Special Issue "Modern and fossil oceanic lithosphere"*, 31: 207-221.
- Ullemeyer K., Spalthoff P., Heinitz J., Isakov N.N., Nikitin A.N. and Weber K., 1998. The SKAT texture diffractometer at the pulsed reactor IBR-2 at Dubna: experimental layout and first measurements. *Nuclear Instrum. Methods Physics Res., A*, 412: 80-88.
- Warren J.M. and Shimizu N., 2010. Cryptic variations in abyssal peridotite compositions: evidence for shallow-level melt infiltration in the oceanic lithosphere. *J. Petrol.*, 51: 395-423.
- Warren J.M., Hirth G. and Kelemen P.B., 2008. Evolution of olivine lattice preferred orientation during simple shear in the mantle. *Earth Planet. Sci. Lett.*, 272: 501-512.
- Wenk H.R., 1985. Preferred orientation in deformed metals and rocks; an introduction to modern texture analysis. Orlando, FL, United States. Acad. Press, 610 pp.
- Wenk H-R., 1991. Standard project for pole figure determination by neutron diffraction. *J. Appl. Crystall.*, 24: 920-927.
- Wenk H.R., Matthies S. and Lutterotti L., 1994. Texture analysis from diffraction spectra. *Materials Sci. Forum*, 157: 473-480.
- Wetzel R., 1972. Zur Petrographie und Mineralogie der Furgg-Zone (Monte Rosa-Decke). *Schweiz. Mineral. Petrogr. Mitt.*, 52: 161-236.
- Wicks F.J. and O'Hanley D.S., 1988. Serpentine textures and serpentinization. *Can. Mineral.*, 15: 459-488.
- Zucali M., Chateigner D., Dugnani M., Lutterotti L. and Ouladdiaf B., 2002. Quantitative texture analysis of naturally deformed hornblende under eclogite facies conditions (Sesia-Lanzo Zone, Western Alps): comparison between x-ray and neutron diffraction analysis. In: S. De Meer, M.R. Drury, J.H.P. De Bresser, and G.M. Pennock (Eds.), *Deformation mechanisms, rheology and tectonics: current status and future perspectives*. Geol. Soc. London Spec. Publ., 200: 239-253.

Received, September 3, 2011

Accepted, December 7, 2011